Cell Stem Cell

Article

# Nicotinamide phosphoribosyltransferase inhibitors selectively induce apoptosis of AML stem cells by disrupting lipid homeostasis

## Graphical abstract

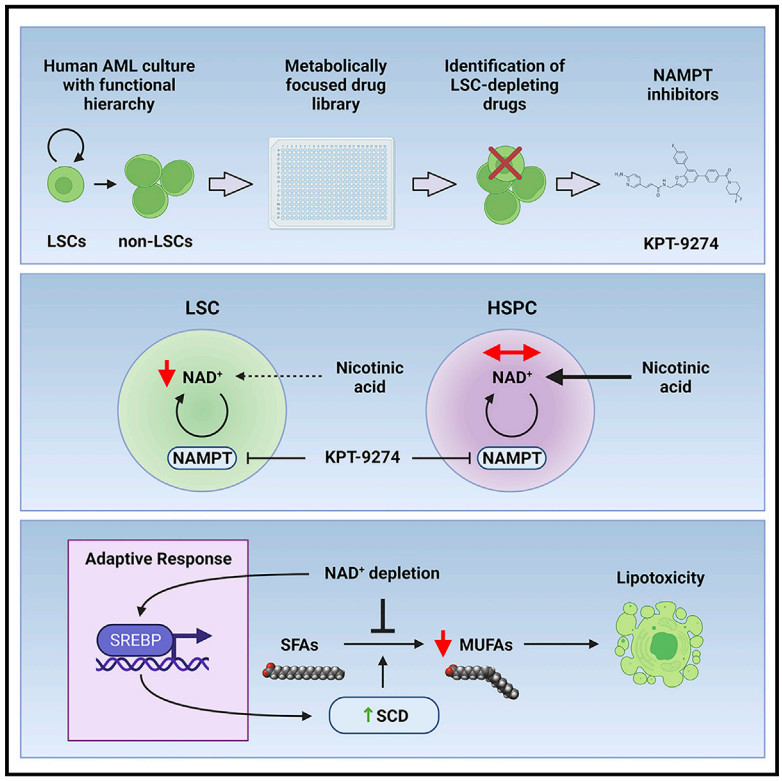


## Highlights

- NAMPT inhibition selectively induces apoptosis of AML stem cells over normal HSCs
- NAD depletion causes lipotoxicity by suppressing the conversion of SFAs to MUFAs
- NAD depletion induces an adaptive lipogenic response coordinated by SREBP2
- Inhibition of SREBP or SCD activity enhances cytotoxicity of NAMPT inhibitors.

## Authors

Amit Subedi, Qiang Liu, Dhanoop M. Ayyathan, ..., Mark D. Minden, Jean C.Y. Wang, Steven M. Chan

## Correspondence

steven.chan@uhnresearch.ca

## In brief

Subedi et al. found that AML stem cells (LSCs) are more dependent on NAMPT activity than normal hematopoietic stem cells for survival. NAMPT inhibition disrupts lipid homeostasis, resulting in lipotoxicity and triggers an adaptive SREBP2-dependent lipogenic response. Suppression of this response enhances the cytotoxicity of NAMPT inhibitors on LSCs.

Subedi et al., 2021, Cell Stem Cell *28*, 1–17
October 7, 2021 
https://doi.org/10.1016/j.stem.2021.06.004

CellPress

Please cite this article in press as: Subedi et al., Nicotinamide phosphoribosyltransferase inhibitors selectively induce apoptosis of AML stem cells by disrupting lipid homeostasis, Cell Stem Cell (2021), https://doi.org/10.1016/j.stem.2021.06.004

Cell Stem Cell

CellPress

Article

# Nicotinamide phosphoribosyltransferase inhibitors selectively induce apoptosis of AML stem cells by disrupting lipid homeostasis

Amit Subedi,[1] Qiang Liu,[1] Dhanoop M. Ayyathan,[1] David Sharon,[1] Severine Cathelin,[1] Mohsen Hosseini,[1] Changjiang Xu,[1,2] Veronique Voisin,[1,2] Gary D. Bader,[1,2] Angelo D'Alessandro,[3] Eric R. Lechman,[1] John E. Dick,[1,4] Mark D. Minden,[1,5,6] Jean C.Y. Wang,[1,5,6] and Steven M. Chan[1,5,6,7,*]

[1]Princess Margaret Cancer Centre, University Health Network, Toronto, ON, Canada
[2]Donnelly Centre for Cellular and Biomolecular Research, Toronto, ON, Canada
[3]Department of Biochemistry and Molecular Genetics, University of Colorado Denver, Aurora, CO, USA
[4]Department of Molecular Genetics, University of Toronto, Toronto, ON, Canada
[5]Department of Medicine, University of Toronto, ON, Canada
[6]Division of Medical Oncology and Hematology, Department of Medicine, University Health Network, Toronto, ON, Canada
[7]Lead contact
*Correspondence: steven.chan@uhnresearch.ca
https://doi.org/10.1016/j.stem.2021.06.004

## SUMMARY

Current treatments for acute myeloid leukemia (AML) are often ineffective in eliminating leukemic stem cells (LSCs), which perpetuate the disease. Here, we performed a metabolic drug screen to identify LSC-specific vulnerabilities and found that nicotinamide phosphoribosyltransferase (NAMPT) inhibitors selectively killed LSCs, while sparing normal hematopoietic stem and progenitor cells. Treatment with KPT-9274, a NAMPT inhibitor, suppressed the conversion of saturated fatty acids to monounsaturated fatty acids, a reaction catalyzed by the stearoyl-CoA desaturase (SCD) enzyme, resulting in apoptosis of AML cells. Transcriptomic analysis of LSCs treated with KPT-9274 revealed an upregulation of sterol regulatory-element binding protein (SREBP)-regulated genes, including *SCD,* which conferred partial protection against NAMPT inhibitors. Inhibition of SREBP signaling with dipyridamole enhanced the cytotoxicity of KPT-9274 on LSCs *in vivo*. Our work demonstrates that altered lipid homeostasis plays a key role in NAMPT inhibitor-induced apoptosis and identifies NAMPT inhibition as a therapeutic strategy for targeting LSCs in AML.

## INTRODUCTION

Acute myeloid leukemia (AML) is an aggressive hematologic malignancy. Although high-intensity chemotherapy as front-line treatment induces morphologic remission in up to 70% of patients (Dombret and Gardin, 2016), disease relapse is a frequent occurrence and is thought to be due to the persistence of disease-sustaining leukemic stem cells (LSCs) (Bonnet and Dick, 1997; Shlush et al., 2017). Novel therapies that eradicate LSCs may lead to more durable responses and improve outcomes.

One of the keys to the development of more effective AML therapies is identification of vulnerabilities that are present in LSCs. Prior studies have demonstrated that LSCs possess metabolic properties and dependencies that are distinct from their more differentiated progenies (henceforth referred to as "non-LSCs") and from normal hematopoietic stem cells (HSCs) (Ito and Suda, 2014; Jones et al., 2018; Lagadinou et al., 2013). These metabolic differences can be exploited for therapeutic purposes. For instance, LSCs have been shown to be more dependent on oxidative phosphorylation (OXPHOS) than HSCs (Lagadinou et al., 2013), an observation that has led to the study of a variety of mitochondrial inhibitors as potential anti-LSC agents (Molina et al., 2018; Skrtić et al., 2011). This approach is exemplified by venetoclax, which has been shown to target LSCs through its ability to suppress electron transport chain (ETC) activity and the tricarboxylic acid (TCA) cycle (Jones et al., 2018; Pollyea et al., 2018; Sharon et al., 2019). LSCs are also reported to maintain lower levels of reactive oxygen species (ROS) than non-LSCs (Lagadinou et al., 2013) and are more susceptible to agents that induce oxidative stress (Guzman et al., 2005). Furthermore, some driver mutations in AML that promote stemness properties (e.g., isocitrate dehydrogenase [*IDH*] mutations) have been shown to dysregulate metabolic pathways and confer druggable vulnerabilities that are not present in unmutated cells (Chan et al., 2015). Taken together, LSCs appear to be more dependent on certain metabolic processes for their survival than non-LSCs and normal HSCs. Yet our understanding of the differences in metabolic dependencies among the various cell types is incomplete. Identification of additional LSC-specific metabolic vulnerabilities could offer new therapeutic opportunities.

Please cite this article in press as: Subedi et al., Nicotinamide phosphoribosyltransferase inhibitors selectively induce apoptosis of AML stem cells by disrupting lipid homeostasis, Cell Stem Cell (2021), https://doi.org/10.1016/j.stem.2021.06.004



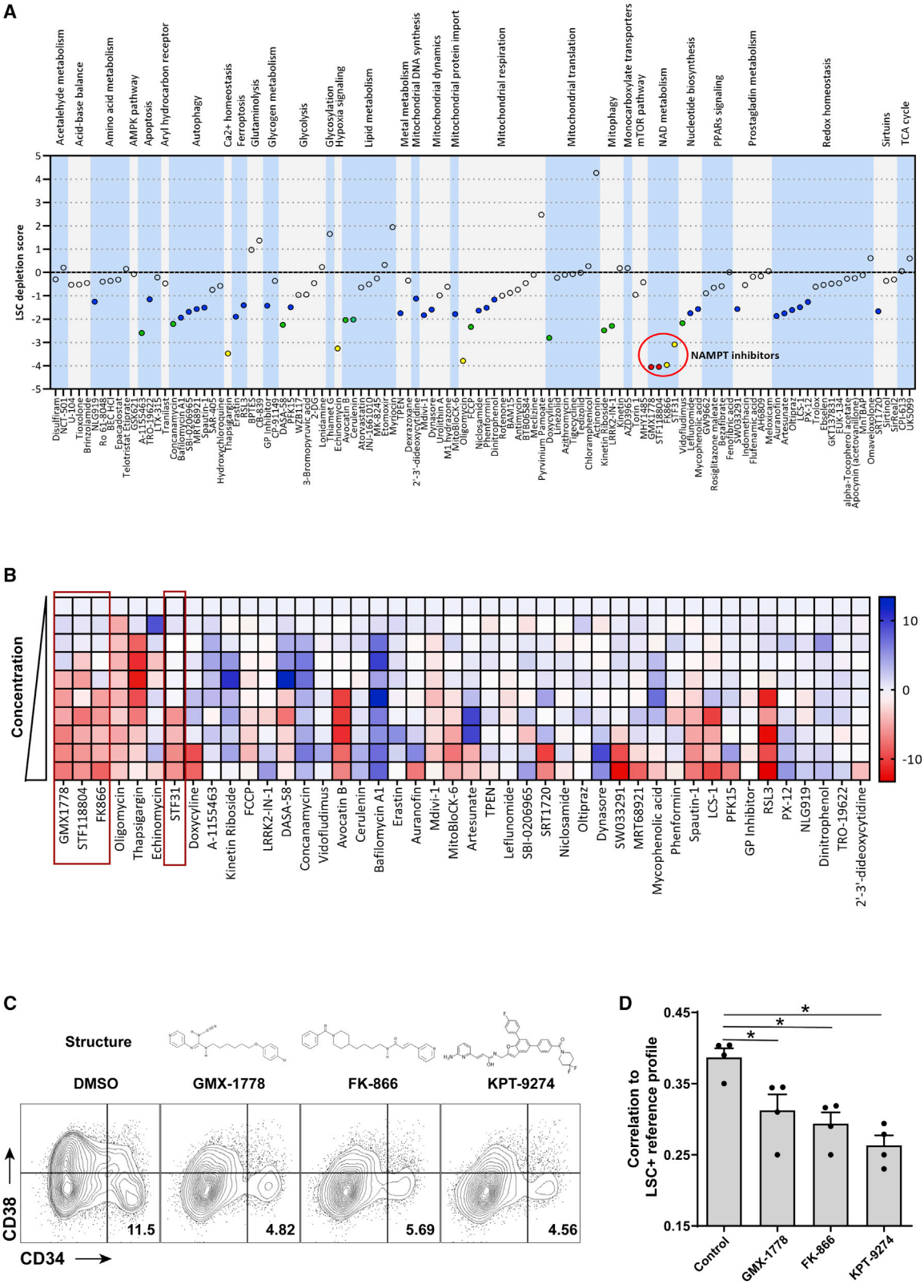


*(legend on next page)*

Please cite this article in press as: Subedi et al., Nicotinamide phosphoribosyltransferase inhibitors selectively induce apoptosis of AML stem cells by disrupting lipid homeostasis, Cell Stem Cell (2021), https://doi.org/10.1016/j.stem.2021.06.004



To address the above issues, we performed a metabolic drug screen to identify compounds with anti-LSC activity and identified nicotinamide phosphoribosyltransferase (NAMPT) inhibitors as potential hits. NAMPT catalyzes the rate-limiting step in the nicotinamide adenine dinucleotide ($NAD^+$) salvage pathway and has previously been identified as a therapeutic target in several cancer types, including colorectal (Zhang et al., 2013), ovarian (Nacarelli et al., 2020), breast (Zhang et al., 2019a), gliomas (Zhang et al., 2012), T cell lymphomas (Kozako et al., 2019), and AML (Cagnetta et al., 2015; Jones et al., 2020; Mitchell et al., 2019). However, most of these studies examined the impact of NAMPT inhibition on the bulk cancer population, and thus our understanding of its impact on the malignant stem cell population is limited. Additionally, it is not clear whether malignant stem cells and their normal stem cell counterparts are differentially dependent on NAMPT activity for their survival. Furthermore, the precise mechanisms by which NAMPT inhibition induces cell death have not been thoroughly explored. In this study, we addressed these issues in the context of AML stem cells and discovered that disruption of lipid homeostasis plays a critical role in mediating NAMPT inhibitor-induced cell death.

## RESULTS

### Drug screen identifies NAMPT inhibitors as candidate anti-LSC compounds

To identify metabolic drugs with anti-LSC activity, we curated a library of 110 compounds that have previously been characterized to affect metabolic enzymes, processes, or pathways (Table S1). We applied this library to screen for compounds that depleted LSCs in a previously established human AML culture, known as OCI-AML-8227 (Lechman et al., 2016). In OCI-AML-8227, LSCs assayed by xenotransplantation are restricted to the $CD34^+CD38^-$ fraction, while the $CD34^+CD38^+$ fraction is enriched for clonogenic progenitors and the $CD34^-$ fraction for terminally differentiated blasts (Kaufmann et al., 2019; Lechman et al., 2016). Importantly, the CD34/CD38 profile and hierarchical organization are maintained in culture. Gene expression analysis of the $CD34^+CD38^-$ fraction from OCI-AML-8227 demonstrated a strong correlation between the expression of 104 genes associated with LSC activity and a $LSC^+$ reference profile (Kaufmann et al., 2019; Ng et al., 2016). These findings support the use of OCI-AML-8227 for the identification of compounds with anti-LSC activity on the basis of their ability to deplete $CD34^+CD38^-$ cells.

In the primary screen, we treated OCI-AML-8227 with each compound at eight different concentrations for 3 days and then measured the total number of viable cells and proportion of $CD34^+CD38^-$ cells using flow cytometry. A composite LSC depletion score based on the relative reduction in the $CD34^+CD38^-$ fraction across the eight different concentrations was calculated for each compound, with a lower score representing a more effective compound (Figure 1A; Table S1). Several compounds that have previously been shown to target cancer stem cells, including oligomycin (Viale et al., 2014), echinomycin (Wang et al., 2011), thapsigargin (Biddle et al., 2016), doxycycline (Matsumoto et al., 2017), and avocatin B (Lee et al., 2015), were among the top hits, thereby providing internal validation of the screen. Strikingly, the top 3 hits and 7th ranked hit were all structurally unrelated NAMPT inhibitors (GMX-1778, STF-118804, FK-866, and STF-31) (Galli et al., 2020; Ogino et al., 2018). Next, we conducted a secondary screen using the top 44 hits from the primary screen and validated the anti-LSC activity of most compounds, including the four NAMPT inhibitors (Figure 1B; Table S1). Treatment of OCI-AML-8227 with KPT-9274, another structurally unrelated NAMPT inhibitor, also depleted the LSC-enriched $CD34^+CD38^-$ fraction (Figure 1C). Moreover, treatment with NAMPT inhibitors reduced the correlation between the above-mentioned LSC gene signature and the $LSC^+$ reference profile (Figure 1D). Taken together, these findings show that NAMPT inhibitors are active against LSCs. NAMPT as a potential therapeutic target is further supported by the observations that (1) human AML samples express higher levels of *NAMPT* than normal hematopoietic stem and progenitor cells (HSPCs) (Figure S1A), and (2) higher *NAMPT* expression in AML is associated with worse overall survival (Figure S1B).

### LSCs are more susceptible to apoptosis from NAMPT inhibition than non-LSCs

We decided to focus on KPT-9274 for our subsequent studies because it is the furthest along in clinical development among NAMPT inhibitors. KPT-9274 was initially identified on the basis of its ability to inhibit the P21 activated kinase 4 (PAK4) protein and was subsequently found also to block NAMPT activity (Abu Aboud et al., 2016). To determine if the impact of KPT-9274 on LSCs was due to NAMPT inhibition, we performed rescue experiments by adding the $NAD^+$ precursor, nicotinamide riboside (NR). After cellular uptake, NR is phosphorylated to become nicotinamide mononucleotide (NMN), which is the product of the reaction catalyzed by NAMPT (Figure S2A). Addition of NR rescued the $CD34^+CD38^-$ population in OCI-AML-8227 treated with KPT-9274, indicating that the effect was dependent on NAMPT inhibition (Figure S2B).

We tested the impact of KPT-9274 on another patient-derived AML cell culture known as OCI-AML-21. Like OCI-AML-8227, LSC activity assayed by xenotransplantation was restricted to

**Figure 1. Drug screen identifies NAMPT inhibitors as candidate anti-LSC compounds**

(A) Composite LSC depletion score for each of the 110 compounds in the primary screen against OCI-AML-8227. Scores less than 0 indicate a decrease in size of the $CD34^+CD38^-$ population.

(B) Heatmap of *t* values for the indicated compound at ten different concentrations. Data shown are from the secondary screen of the top 44 hits from primary screen. Values less than 0 indicate a decrease in size of the $CD34^+CD38^-$ population in OCI-AML-8227.

(C) CD34 and CD38 expression profile of OCI-AML-8227 after treatment with the NAMPT inhibitor GMX-1778 (20 nM), FK-866 (10 nM), or KPT-9274 (1.5 μM) for 3 days. Representative data from three independent experiments.

(D) Spearman's correlation coefficient between the expression profile of 104 genes associated with LSC activity in OCI-AML-8227 after treatment with the indicated compounds and the $LSC^+$ reference profile. n = 4 independent experiments. Data shown are mean ± SEM. Statistical significance was determined using Student's t test. *$p \leq 0.05$.

See also Figure S1.

Please cite this article in press as: Subedi et al., Nicotinamide phosphoribosyltransferase inhibitors selectively induce apoptosis of AML stem cells by disrupting lipid homeostasis, Cell Stem Cell (2021), https://doi.org/10.1016/j.stem.2021.06.004



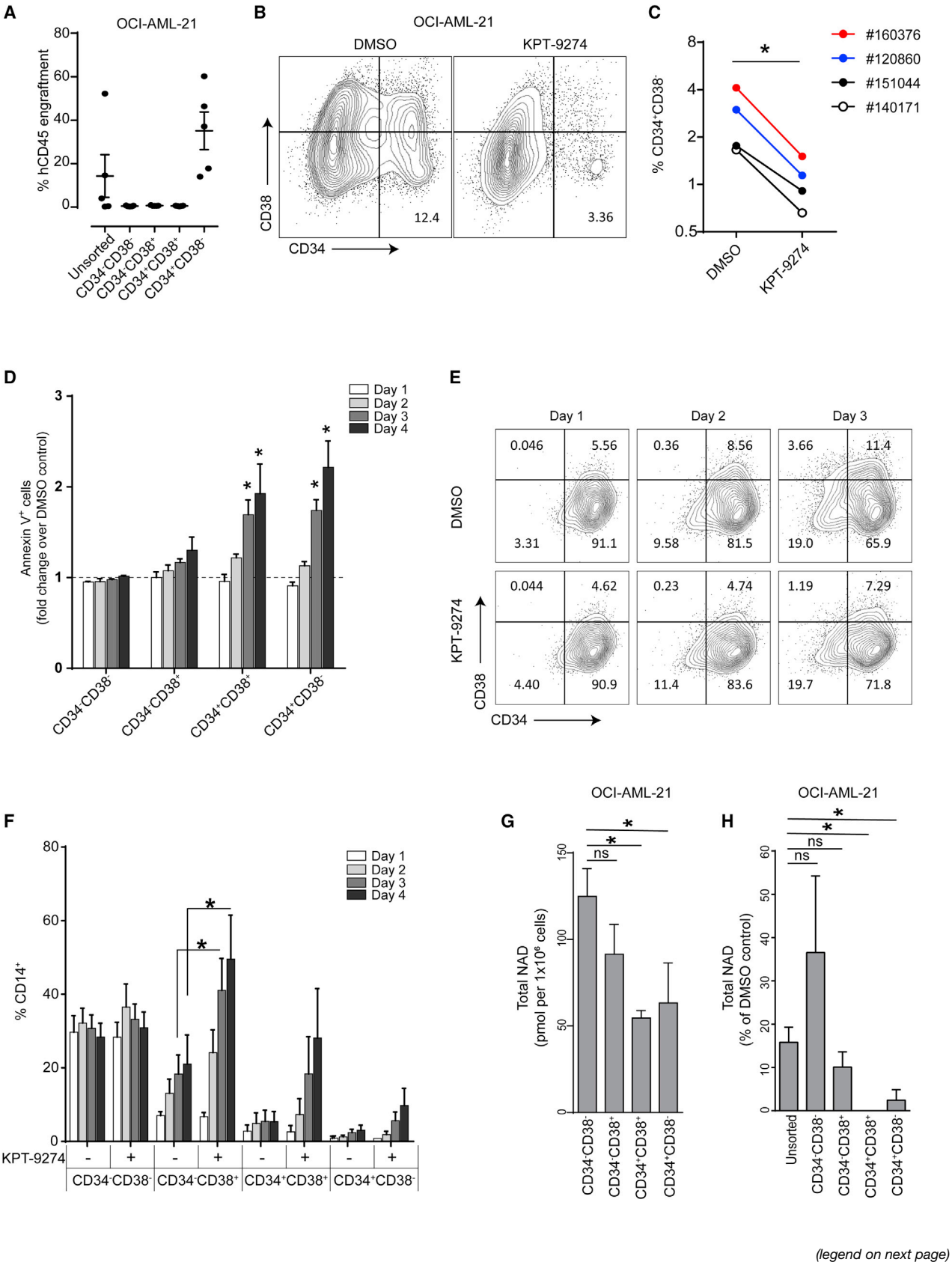


(legend on next page)

Please cite this article in press as: Subedi et al., Nicotinamide phosphoribosyltransferase inhibitors selectively induce apoptosis of AML stem cells by disrupting lipid homeostasis, Cell Stem Cell (2021), https://doi.org/10.1016/j.stem.2021.06.004



the $CD34^+CD38^-$ fraction in OCI-AML-21 (Figure 2A). The LSC 104-gene signature of this cell fraction was more correlated with the $LSC^+$ reference profile than that of the other fractions (Figure S2C). Treatment of OCI-AML-21 with KPT-9274 for 3 days decreased the size of the $CD34^+CD38^-$ fraction (Figure 2B). We treated four primary AML patient samples with KPT-9274 in short term *ex vivo* cultures and similarly observed a reduction in their $CD34^+CD38^-$ fractions (Figures 2C and S2D). These findings suggest that LSCs are broadly sensitive to NAMPT inhibition.

The selective depletion of $CD34^+CD38^-$ cells could be attributed to either a higher susceptibility to cell death or enforced differentiation into the non-LSC fractions after drug treatment. To distinguish between these possibilities, we sorted OCI-AML-21 cells into four fractions on the basis of CD34 and CD38 expression and treated each fraction with KPT-9274 for 3–4 days in culture. We observed a progressive increase in apoptotic cells by annexin V staining only in the $CD34^+CD38^-$ and $CD34^+CD38^+$ sorted fractions but not in the more mature $CD34^-$ fractions (Figure 2D). Moreover, KPT-9274 treatment induced cell-cycle arrest at G0/G1 phase in the remaining viable $CD34^+CD38^-$ cells (Figure S2E). In contrast, KPT-9274 treatment had no clear impact on the differentiation state of the remaining viable $CD34^+CD38^-$ sorted cells (Figure 2E). To further investigate its impact on differentiation, we analyzed for changes in CD14 expression, a monocytic differentiation marker, on sorted OCI-AML-21 cells. KPT-9274 treatment increased the expression of CD14 on $CD34^-CD38^+$ cells but not $CD34^+CD38^-$ cells (Figure 2F), indicating that NAMPT inhibition can induce further maturation in differentiated blasts but not in LSCs. Our results indicate that NAMPT inhibitors deplete LSCs primarily through induction of apoptosis.

To determine the basis behind the differential sensitivity to NAMPT inhibitors, we measured total intracellular NAD levels ($NAD^+$ and NADH) in sorted fractions of untreated OCI-AML-8227 and OCI-AML-21. The NAD levels in the $CD34^+$ fractions were lower than those in the $CD34^-$ fractions for both cell lines (Figures 2G and S2F). To determine if the lower NAD levels could be attributed to higher $NAD^+$ consumption, we measured the mRNA levels of different isoforms of poly (ADP-ribose) polymerases (PARPs) and sirtuins (SIRTs), the two major classes of intracellular $NAD^+$-consuming enzymes, in sorted fractions of OCI-AML-21. Expression of *PARP1-3* and *SIRT5* were higher in the $CD34^+$ fractions than in $CD34^-$ fractions (Figure S2G). Analysis of an independent dataset showed that these genes were also more highly expressed in functionally defined $LSC^+$ fractions than in LSC fractions (Ng et al., 2016) (Figure S2H). These findings suggest that the lower NAD levels in $CD34^+$ cells could be due to higher $NAD^+$ consumption. Treatment with KPT-9274 for 24 h (prior to onset of massive apoptosis) reduced NAD levels in all the fractions, but the impact was greatest in the $CD34^+$ fractions, in which levels became almost undetectable after treatment (Figure 2H). This differential dependency on NAMPT activity was not associated with differences in NAMPT protein expression among cells fractions in OCI-AML-21 or OCI-AML-8227 (Figures S2I and S2J). Collectively, these results suggest that $CD34^+$ AML cells, which are enriched for LSCs, are more sensitive to NAMPT inhibition than $CD34^-$ AML cells because of a lower steady-state concentration of NAD and greater dependency on the salvage pathway to sustain NAD levels.

## KPT-9274 selectively targets LSCs over normal HSPCs *in vivo*

As maintenance of an adequate intracellular NAD pool is essential for the survival of all cells, it is critical to determine if a therapeutic window exists for NAMPT inhibitors. Upon inhibition of the salvage pathway, $NAD^+$ can be generated from dietary precursors via alternative pathways including the Preiss-Handler (PH) pathway (Figure S2A). The PH pathway starts with the rate-limiting conversion of dietary nicotinic acid (NA) to NA mononucleotide (NAMN) by the enzyme NA phosphoribosyltransferase (NAPRT). The ability to use the PH pathway for $NAD^+$ generation would sustain the intracellular NAD pool when the salvage pathway is inhibited. To determine if LSCs and normal HSPCs differ in their ability to use the PH pathway, we compared the impact of exogenous NA on KPT-9274 sensitivity in OCI-AML-21, OCI-AML-8227, and $CD34^+$ HSPCs from cord blood (CB). KPT-9274 treatment for 3 days decreased the viability of $CD34^+$ HSPCs (Figure 3A), an effect that was rescued by the addition of NA at a physiologically relevant concentration (100 μM). This finding indicates that the PH pathway can compensate for inhibition of the salvage pathway in $CD34^+$ HSPCs. In contrast, exogenous NA at the same concentration failed to rescue the depletion of $CD34^+CD38^-$ cells in OCI-

**Figure 2. LSCs are more susceptible to apoptosis from NAMPT inhibition than non-LSCs**

(A) Human engraftment in BM of NSG mice transplanted intrafemorally with the indicated fractions of OCI-AML-21 at 13 weeks post-transplantation. Each data point represents an individual animal. n = 5 mice per group.

(B) CD34 and CD38 expression profile of OCI-AML-21 treated with DMSO or KPT-9274 (1.5 μM) for 3 days. Representative data from three independent experiments.

(C) Percentage of $CD34^+CD38^-$ cells in primary AML patient samples treated with DMSO or KPT-9274 (1.5 μM) for 3 days in culture. Statistical significance was determined using paired Student's t test.

(D) Fold change in annexin $V^+$ cells in sorted fractions of OCI-AML-21 treated with KPT-9274 (1.5 μM) over DMSO-treated controls on days 1–4 after treatment. n = 3 independent experiments. Statistical significance was determined using one-way ANOVA.

(E) CD34 and CD38 expression profile of sorted $CD34^+CD38^-$ OCI-AML-21 cells treated with DMSO or KPT-9274 (1.5 μM) on days 1–3 after treatment. Representative data from three independent experiments.

(F) Percentage of $CD14^+$ cells in sorted fractions of OCI-AML-21 treated with DMSO (−) or KPT-9274 (+) at 1.5 μM on days 1–4 after treatment. n = 3 independent experiments.

(G) Total NAD levels in the indicated sorted fractions of untreated OCI-AML-21. n = 3 independent experiments.

(H) Change in total NAD levels in the indicated sorted fractions of OCI-AML-21 after treatment with KPT-9274 (1.5 μM) for 24 h relative to DMSO-treated cells. n = 3 independent experiments.

Data shown are mean ± SEM. Unless otherwise noted, statistical significance was determined using unpaired two-tailed Student's t test. *p ≤ 0.05. See also Figure S2.

Please cite this article in press as: Subedi et al., Nicotinamide phosphoribosyltransferase inhibitors selectively induce apoptosis of AML stem cells by disrupting lipid homeostasis, Cell Stem Cell (2021), https://doi.org/10.1016/j.stem.2021.06.004



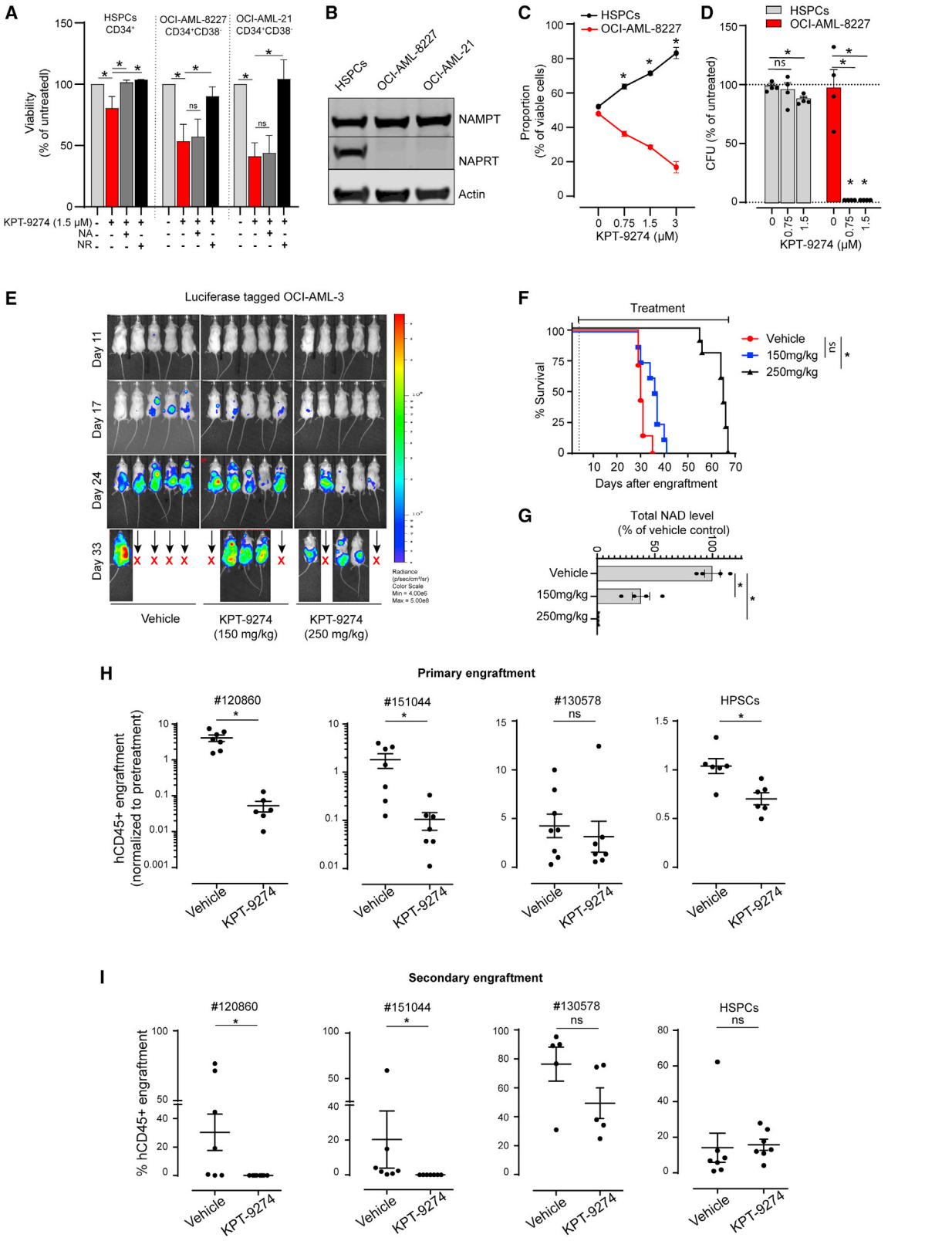


(legend on next page)

Please cite this article in press as: Subedi et al., Nicotinamide phosphoribosyltransferase inhibitors selectively induce apoptosis of AML stem cells by disrupting lipid homeostasis, Cell Stem Cell (2021), https://doi.org/10.1016/j.stem.2021.06.004



AML-21 and OCI-AML-8227 (Figure 3A), suggesting that the PH pathway is not functional in LSCs. In support of these findings, NAPRT was expressed only in $CD34^+$ HSPCs and not in OCI-AML-8227 and OCI-AML-21 (Figure 3B). Exogenous NR rescued the decrease in viability in all three cell types, thus confirming target specificity (Figure 3A).

To directly compare the relative toxicity of KPT-9274 against AML cells versus normal HSPCs, we performed a growth competition assay between blue fluorescent protein (BFP)-tagged OCI-AML-8227 cells and $CD34^+$ HSPCs from CB. The two cell types were mixed at a 1:1 ratio and treated with KPT-9274 at different concentrations in the presence of NA. KPT-9274 treatment decreased the proportion of AML ($BFP^+$) cells in the viable fraction in a dose dependent manner (Figure 3C) and induced more apoptosis in AML cells than HSPCs (Figure S3A). KPT-9724 treatment also reduced the clonogenic capacity of OCI-AML-8227 to a greater extent than that of HSPCs in methylcellulose medium containing NA (Figure 3D). On the basis of these findings, we postulated that NAMPT inhibitors can selectively target LSCs while sparing HSPCs because of their differential capacity to use the PH pathway for $NAD^+$ generation.

To test our hypothesis *in vivo*, we transplanted OCI-AML-3 AML cells engineered to stably express firefly luciferase into sub-lethally irradiated NOD/SCID/IL2R$\gamma^{-/-}$ (NSG) mice. After confirmation of engraftment by bioluminescence imaging on day 4 post-transplantation, we started treatment with vehicle or KPT-9274 at a dose of 150 or 250 mg/kg per day by oral administration. KPT-9274 treatment at 250 mg/kg decreased disease burden (Figures 3E and S3B) and prolonged survival (Figure S3C) compared with controls. Treatment at the lower dose was less effective in reducing leukemic burden and failed to improve survival. To confirm these findings, we repeated this experiment by directly measuring leukemic burden in bone marrow (BM) samples using flow cytometry. Consistent with the previous experiment, KPT-9274 treatment at 250 mg/kg, but not at 150 mg/kg, significantly reduced leukemic burden at days 20 and 29 post-transplantation (Figure S3D) and increased survival (Figure 3F) compared with controls. To determine if treatment efficacy correlated with degree of NAD depletion, we measured the NAD levels in leukemic cells collected from engrafted mice after treatment with vehicle or KPT-9274 at the two different doses for 2 days. Treatment at 150 mg/kg reduced NAD levels to ~40% of control levels, while treatment at 250 mg/kg resulted in an almost complete depletion (Figure 3G), suggesting that NAD depletion beyond a threshold is required to trigger cell death and provides an explanation for the difference in efficacy between the two doses.

Next, we investigated the impact of KPT-9274 treatment in three patient-derived xenograft (PDX) models as well as in NSG mice engrafted with $CD34^+$ HSPCs from CB. The AML samples used to generate the PDX models were collected at diagnosis, prior to treatment initiation (Table S2). After determining the baseline level of human engraftment in BM at 6–8 weeks post-transplantation (Figure S3E), we treated the mice with either vehicle or KPT-9274 at a dose of 150 mg/kg twice a day for 3 weeks on a 5-days-on, 2-days-off schedule. KPT-9274 treatment decreased the leukemia burden from baseline in two of the three PDX models (120860 and 151044) but not in the third PDX model (130578) (Figures 3H and S3F). The proportion of $CD14^+$ cells was higher with KPT-9274 treatment compared with controls in all three PDX models (Figure S3G). KPT-9274 treatment reduced the level of human chimerism by ~25% in mice engrafted with $CD34^+$ HSPCs (Figures 3H and S3F). To determine if LSCs and normal HSCs were targeted, we collected BM cells from the primary recipients at the end of treatment, transplanted equivalent numbers of cells into secondary NSG recipients and determined the level of human engraftment in the BM at 6–7 weeks after transplantation. KPT-9274 treatment abolished the secondary engraftment potential of the two PDX models (120860 and 151044) in which a reduction in leukemic burden was observed in primary recipients (Figure 3I). However,

**Figure 3. KPT-9274 selectively targets LSCs over normal HSPCs *in vivo***

(A) Viability of the indicated cells after treatment with KPT-9274 at 1.5 μM for 3 days in the presence or absence of NA at 100 μM or NR at 100 μM. n = 3 independent experiments.

(B) NAMPT and NAPRT protein expression level in indicated cells by western blot analysis. Representative data from three independent experiments.

(C) Proportion of OCI-AML-8227 ($BFP^+$) cells and HSPCs ($BFP^-$) in a growth competition assay treated with the indicated concentration of KPT-9274 for 3 days. The two cell types were mixed at a 1:1 ratio in medium containing NA at 100 μM at the start of the experiment. n = 3 independent experiments. Statistical comparison is between the proportion of HSPCs treated at the indicated concentration of KPT-9274 and untreated control.

(D) CFUs of OCI-AML-8227 and HSPCs treated with the indicated concentration of KPT-9274 after 7 days in methylcellulose medium containing NA at 100 μM. n = 4 independent experiments.

(E) Leukemic burden as determined by bioluminescence imaging of NSG mice transplanted with luciferase-tagged OCI-AML-3 cells at the indicated time points after transplantation. Treatment with vehicle or KPT-9274 at the indicated dosing was started 4 days after transplantation. n = 5 mice per treatment arm. Quantification results of radiance are shown in Figure S3B.

(F) Survival of NSG mice transplanted with OCI-AML-3 cells. Treatment with vehicle or KPT-9274 at the indicated dosing was started 4 days after transplantation. n = 7–10 mice per treatment arm. Statistical significance was determined using log rank (Mantel-Cox) test compared with vehicle-treated arm.

(G) Total NAD levels in leukemic cells from BM of NSG mice engrafted with OCI-AML-3 cells and treated with vehicle or KPT-9274 at the indicated dosing for 3 consecutive days. n = 4 mice per treatment arm.

(H) Human engraftment in BM of primary NSG recipients transplanted with the indicated primary AML samples or CB $CD34^+$ HSPCs and treated with vehicle or KPT-9274 at 150 mg/kg twice a day for 3 weeks on a 5-days-on, 2-days-off schedule. Engraftment was confirmed and quantified before starting treatment. Data shown are normalized to the pre-treatment engraftment level for each animal. Values less than 1 are indicative of a reduction in leukemic burden or human engraftment from baseline. Each data point represents an individual mouse. n = 6–8 mice per treatment arm.

(I) Human engraftment in the BM of secondary NSG recipients at 7 weeks after transplantation with equal number of BM cells collected from animals shown in (H). Each data point represents an individual mouse. n = 5–7 mice per arm.

Data shown are mean ± SEM. Unless otherwise noted, statistical significance was determined using unpaired two-tailed Student's t test. *$p \leq 0.05$. See also Figure S3.

Please cite this article in press as: Subedi et al., Nicotinamide phosphoribosyltransferase inhibitors selectively induce apoptosis of AML stem cells by disrupting lipid homeostasis, Cell Stem Cell (2021), https://doi.org/10.1016/j.stem.2021.06.004



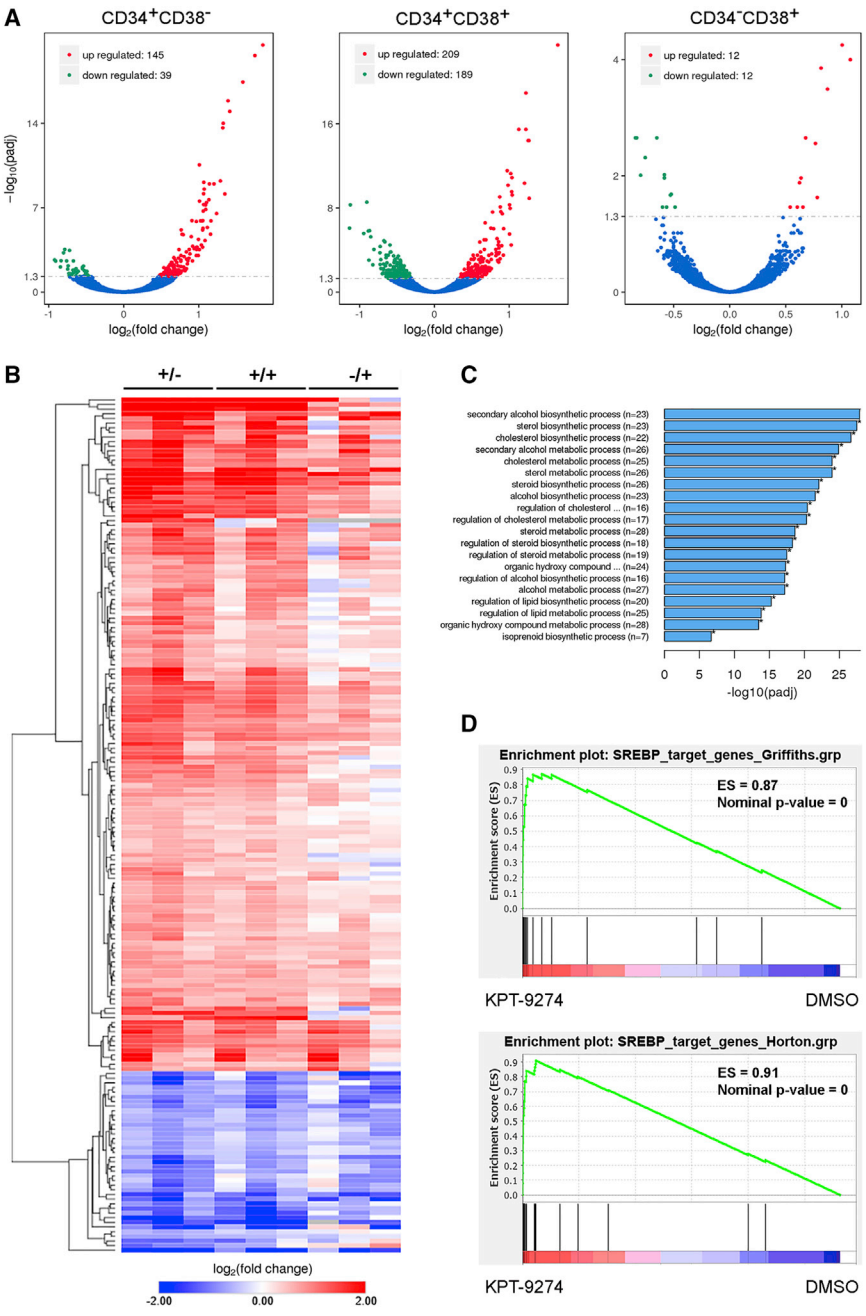


**Figure 4. KPT-9274 treatment upregulates expression of SREBP-regulated genes**

(A) Volcano plots of DEGs in sorted fractions of OCI-AML-21 treated with DMSO versus KPT-9274 at 1.5 μM for 48 h.

(B) Heatmap showing the fold change in expression of the 184 DEGs in $CD34^+CD38^-$ OCI-AML-21 cells after treatment with KPT-9274 relative to DMSO treatment. Changes in expression of the same genes in the other cell fractions are also displayed. Three experimental replicates were performed for each fraction. Each row presents a different gene. Unsupervised hierarchical clustering of the genes was performed.

(C) GO enrichment analysis of the 145 differentially upregulated genes in the $CD34^+CD38^-$ fraction of OCI-AML-21 after treatment with KPT-9274.

(D) GSEA of RNA-seq data generated from the $CD34^+CD38^-$ fraction of OCI-AML-21 after treatment with DMSO or KPT-9274 using two published gene sets of SREBP-regulated genes.

See also Figure S4.

## KPT-9274 treatment upregulates expression of SREBP-regulated genes

We postulated that resistance to NAMPT inhibitors could arise from an adaptive transcriptional response to NAD depletion. To test this hypothesis, we performed RNA sequencing (RNA-seq) analysis of sorted $CD34^+CD38^-$, $CD34^+CD38^+$, and $CD34^-CD38^+$ fractions of OCI-AML-21 after treatment with DMSO (control) or KPT-9274 for 48 h. The $CD34^-CD38^-$ fraction did not yield sufficient material for RNA-seq after KPT-9274 treatment. Using a false discovery rate cut-off of 0.05, we identified a greater number of differentially expressed genes (DEGs) between control and treated samples in the two $CD34^+$ fractions compared with the $CD34^-CD38^+$ fraction (Figure 4A). Most of the DEGs in the $CD34^+$ fractions were upregulated with KPT-9274. Of the 145 upregulated DEGs in the $CD34^+CD38^-$ fraction, 96 (66%) overlapped with those in the $CD34^+CD38^+$ fraction, whereas only 9 (6%) were also upregulated in the $CD34^-CD38^+$ fraction (Figure S4A). Intriguingly, 7 of the 9 genes that were upregulated in all three fractions encode enzymes involved in lipid and cholesterol biosynthesis (*SCD*, *HMGCS1*, *HMGCR*, *ACSS2*, *TM7SF2*, *LSS*, and *DHCR7*) (Figures S4B and S4C). Next, we performed unsupervised hierarchical clustering analysis of the DEGs identified in the $CD34^+CD38^-$ fraction and constructed a heatmap to visualize the results. This analysis showed that most of the changes were also observed in the other non-LSC fractions but to a noticeably lesser degree in the $CD34^-CD38^+$ fraction (Figure 4B). This trend is consistent with our finding that NAD depletion was more

it failed to reduce the secondary engraftment potential of the third PDX model (130578) (Figure 3I), despite the increase in $CD14^+$ cells (Figure S3G). This finding is consistent with our earlier results showing that the pro-differentiation effect of KPT-9274 was restricted to $CD34^-CD38^+$ cells but not the LSC-enriched $CD34^+CD38^-$ fraction (Figures 2E and 2F). KPT-9274 did not impair the secondary engraftment potential of normal HSCs (Figure 3I). Overall, the animal studies demonstrate that KPT-9274 treatment targets LSCs while sparing normal HSCs *in vivo*. However, our results also reveal the existence of mechanisms that protect LSCs from the cytotoxicity of NAMPT inhibitors.

Please cite this article in press as: Subedi et al., Nicotinamide phosphoribosyltransferase inhibitors selectively induce apoptosis of AML stem cells by disrupting lipid homeostasis, Cell Stem Cell (2021), https://doi.org/10.1016/j.stem.2021.06.004





pronounced in $CD34^+$ cells than in $CD34^-$ cells after KPT-9274 treatment (Figure 2H).

To gain insights into the biological pathways represented by the DEGs, we performed Gene Ontology (GO) enrichment analysis of the 145 upregulated transcripts identified in the $CD34^+CD38^-$ fraction and found that process terms related to lipid and cholesterol biosynthesis were highly enriched (Figure 4C). This finding, along with the common characteristics of the overlapping DEGs between the three fractions (Figure S4A), suggests that changes in lipid metabolism might be involved in the adaptive response to NAD depletion. Sterol regulatory-element binding proteins (SREBPs), encoded by the genes *SREBF1* and *SREBF2*, are master transcription factors that induce the expression of genes involved in sterol and fatty acid synthesis (Horton et al., 2002). To test if the DEGs associated with KPT-9274 treatment were enriched for known targets of SREBPs, we performed gene set enrichment analysis (GSEA) on the gene expression data of $CD34^+CD38^-$ cells using two published gene sets. The first gene set consists of 17 genes that are downregulated by combined silencing of *SREBF1* and *SREBF2* (Griffiths et al., 2013). The second gene set consists of 24 genes that are upregulated in the liver of mice transgenic for *SREBF1* or *SREBF2* (Horton et al., 2003). GSEA revealed significant positive enrichment of SREBP target genes in the treated samples for both gene sets (Figure 4D). Consistent with these findings, *SREBF2* expression was significantly increased in the drug treated $CD34^+$ samples (Figure S4C). Our results indicate that AML cells including LSCs upregulate the expression of SREBP-regulated genes in response to KPT-9274 treatment.

## Induction of SREBP-regulated genes protects AML cells from NAMPT inhibition

We hypothesized that activation of the lipogenic response is protective against NAD depletion in AML cells. To determine if this transcriptional response occurs in other AML cells, we measured the effect of KPT-9274 treatment on the expression of two well-characterized SREBP target genes, *ACSS2* and *HMGCS1*, in six AML cell lines with half maximal inhibitory concentrations ($IC_{50}$) ranging from 52.5 to 307.6 nM (Figure S5A). KPT-9274 increased the expression of both genes in all six cell lines, with THP-1 showing the greatest response (Figure S5B). Expression of two other known SREBP target genes, *SCD* and *HMGCR*, were also increased in THP-1 cells (Figure S5C). The increase in gene expression was confirmed at the protein level (Figure S5D). Treatment with the structurally distinct NAMPT inhibitor, FK-866, also induced the expression of *ACSS2*, *HMGCR*, and *SCD*, thus arguing against an off-target effect of KPT-9274 (Figure S5E). Furthermore, KPT-9274 treatment increased the expression of both the full-length and cleaved, active forms of SREBP2 in THP-1 cells (Figure S5F), whereas SREBP1 protein expression was undetectable (data not shown). To determine if this response also occurs in primary samples, we measured the change in expression of *ACSS2*, *HMGCR*, *HMGCS1*, and *SCD* at the mRNA and protein levels in 11 primary AML samples across different cytogenetic and mutation profiles (Table S2). KPT-9274 treatment induced expression of the four genes at the mRNA and protein levels in most samples (Figures 5A and S5G). These results suggest that induction of SREBP-regulated genes is a common response to NAMPT inhibition in AML cells.

To determine the role of SREBPs in the regulation of sensitivity to KPT-9274, we transduced THP-1 cells with lentiviral vectors expressing validated short hairpin RNAs (shRNAs) against *SREBF1* or *SREBF2* under a doxycycline-inducible promoter (Figure S5H) and green fluorescent protein (GFP) under a constitutive promoter. Transduced ($GFP^+$) THP-1 cells were sorted and mixed with untransduced ($GFP^-$) cells in a growth competition assay. The mixed populations were treated with doxycycline for 2 days to induce shRNA expression followed by treatment with DMSO (control) or KPT-9274 for 2 more days. KPT-9274 reduced the proportion of cells expressing *SREBF2* shRNAs compared with control treatment (Figure 5B). In contrast, KPT-9274 had no impact on the proportion of cells expressing non-targeting (NT) or *SREBF1* shRNAs (Figure 5B). To test if SREBP2 inhibition can overcome resistance to KPT-9274, we silenced *SREBF2* expression using one of the lentiviral shRNA vectors in primary AML sample 130578, which demonstrated resistance to single agent KPT-9274 treatment *in vivo* (Figures 3H and 3I). KPT-9274 preferentially depleted the $GFP^+$ population expressing *SREBF2* shRNA but not cells expressing NT shRNA (Figure 5B). These findings indicate that the transcriptional response regulated by SREBP2 promotes resistance to KPT-9274 in AML.

To uncover the metabolic basis of this protective effect, we measured the levels of 151 metabolites including lipids in THP-1 cells treated with KPT-9274 for 24 h using a mass spectrometry-based approach. We observed both upregulation and downregulation of metabolites involved in a variety of processes and pathways, including amino acid metabolism, purine/pyrimidine metabolism, the glycolytic pathway, the pentose phosphate pathway, and the TCA cycle (Figure 5C; Table S3). Consistent with the mechanism of action of KPT-9274, $NAD^+$ was the most significantly downregulated metabolite. Of particular relevance to the SREBP response was the depletion of the monounsaturated fatty acids (MUFAs), myristoleic acid ($C14{:}1\Delta^9$), palmitoleic acid ($C16{:}1\Delta^9$), and oleic acid ($C18{:}1\Delta^9$) (OA), which were among the top-ranked downregulated metabolites (Figure 5C). All three MUFAs are products of the stearoyl-CoA desaturase (SCD) enzyme, which catalyzes the desaturation of saturated fatty acids (SFAs), including myristic (C14:0), palmitic (C16:0), and stearic acid (C18:0), at the ninth carbon from the carboxylic end in a NADPH-dependent reaction (Figure 5D). Given that NADP(H) is synthesized from NAD, we reasoned that the depletion of MUFAs could be due to a reduction in SCD enzymatic activity. In support of this hypothesis, we found that KPT-9274 decreased the ratio of MUFAs to SFAs of different carbon lengths (Figure 5E). A reduction in the ratio of MUFAs to SFAs has previously been shown to induce apoptosis through a process termed lipotoxicity (Listenberger et al., 2003; Young et al., 2013). To determine if this process might contribute to cell death induced by KPT-9274, we added exogenous OA (a monounsaturated FA) to THP-1 cells treated with KPT-9274 and found that it effectively blocked cell death (Figure 5F), whereas exogenous palmitic acid (a saturated FA) exacerbated cell death (Figure S5I). The levels of mevalonate and phosphomevalonate were not reduced by KPT-9274 treatment (Table S3), and exogenous cholesterol or other intermediates in the cholesterol synthesis pathway all failed to prevent cell death induced by KPT-9274 (Figure S5I), thus arguing against depletion of these cholesterol metabolites as a contributing factor. These results indicate that

Please cite this article in press as: Subedi et al., Nicotinamide phosphoribosyltransferase inhibitors selectively induce apoptosis of AML stem cells by disrupting lipid homeostasis, Cell Stem Cell (2021), https://doi.org/10.1016/j.stem.2021.06.004



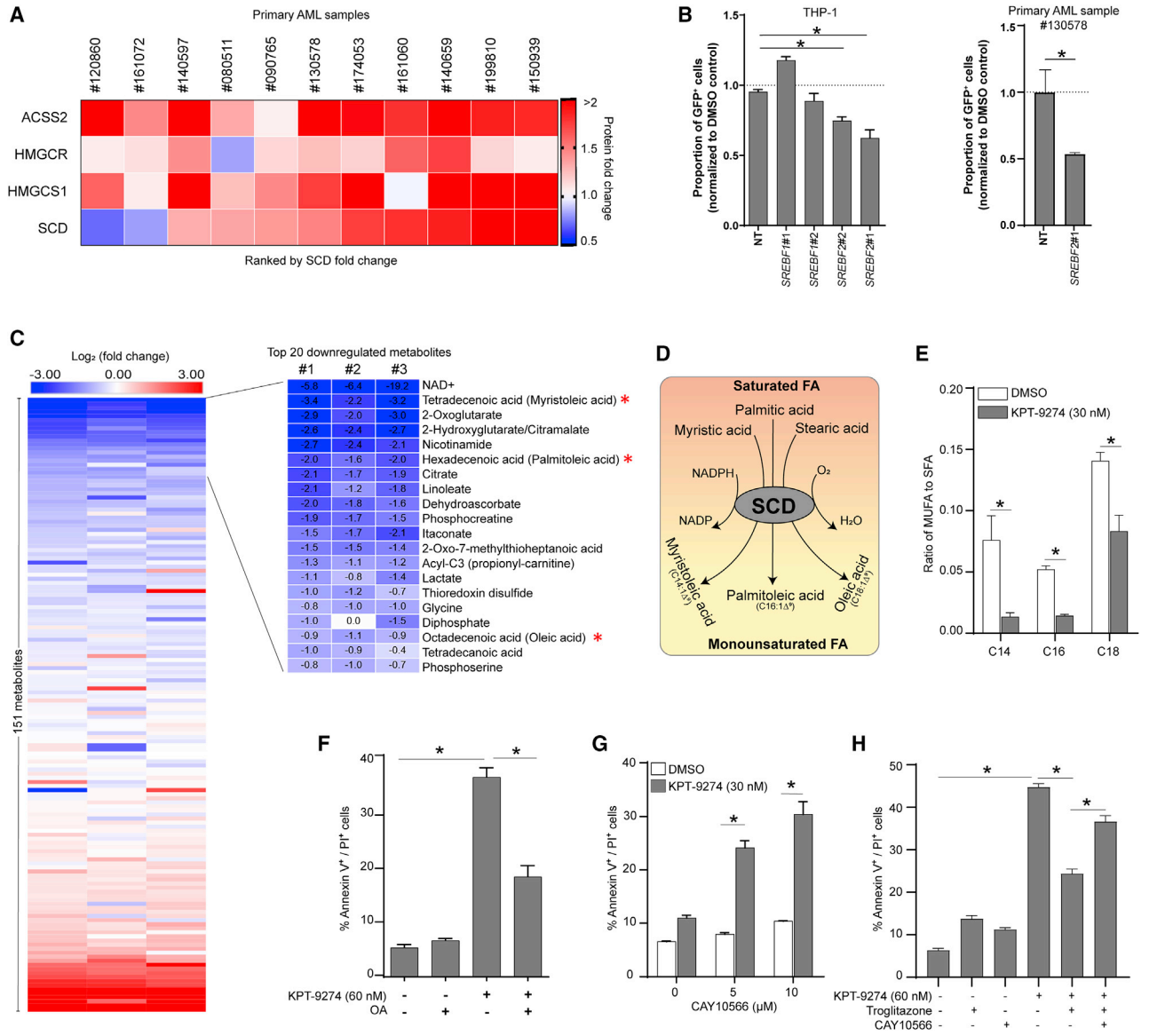


**Figure 5. Induction of SREBP-regulated genes protects AML cells from NAMPT inhibition**

(A) Heatmap showing the fold change in expression of the indicated proteins in 11 primary AML samples after treatment with KPT-9274 at 1 μM for 48 h relative to DMSO treatment.

(B) Proportion of transduced (GFP$^+$) THP-1 or primary AML cells (sample 130578) expressing the indicated shRNAs after induction of shRNA expression with doxycycline (0.25 μg/mL) for 48 h followed by treatment with DMSO or KPT-9274 (30 nM for THP-1 and 0.75 μM for sample 130578) for an additional 48 h. Values are normalized to the proportion of GFP$^+$ cells in DMSO-treated samples. n = 3 independent experiments.

(C) Heatmap showing the fold change in abundance of 151 metabolites in THP-1 cells after treatment with KPT-9274 at 30 nM for 24 h relative to DMSO treatment. The inset shows the top 20 downregulated metabolites after treatment with KPT-9274. n = 3 independent experiments. The metabolites highlighted with an asterisk are MUFAs.

(D) Schematic diagram showing the reactions catalyzed by SCD.

(E) Ratio of MUFA to SFA of different carbon lengths in THP-1 cells treated with DMSO or KPT-9274, as determined by the metabolomic analysis shown in (C). n = 3 independent experiments.

(F) Percentage of dead THP-1 cells treated with KPT-9274 in the presence or absence of OA (75 μM) for 48 h. OA was added 1 h prior to treatment with KPT-9274. n = 3 independent experiments.

(G) Percentage of dead THP-1 cells treated with DMSO or KPT-9274 in the presence or absence of the SCD inhibitor CAY10566 at the indicated concentration for 48 h. CAY10566 was added 1 h prior to treatment with KPT-9274. n = 3 independent experiments.

(H) Percentage of dead THP-1 cells treated with the indicated drugs for 48 h. Troglitazone (50 μM) and CAY10566 (5 μM) were added 1 h prior to treatment with KPT-9274. n = 3 independent experiments.

Data shown are mean ± SEM. Unless otherwise noted, statistical significance was determined using unpaired two-tailed Student's t test. *p ≤ 0.05. See also Figure S5.

Please cite this article in press as: Subedi et al., Nicotinamide phosphoribosyltransferase inhibitors selectively induce apoptosis of AML stem cells by disrupting lipid homeostasis, Cell Stem Cell (2021), https://doi.org/10.1016/j.stem.2021.06.004





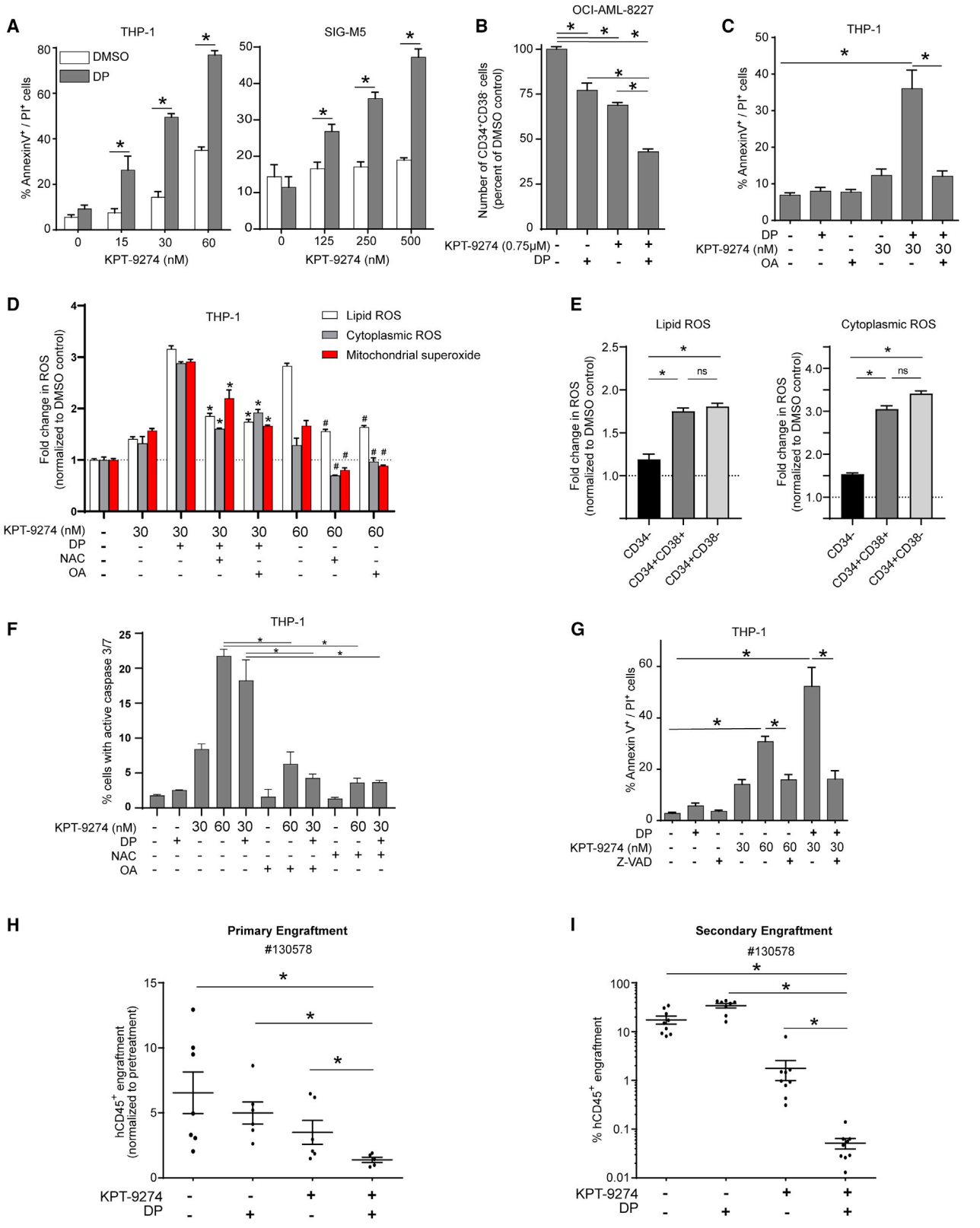


*(legend on next page)*

Please cite this article in press as: Subedi et al., Nicotinamide phosphoribosyltransferase inhibitors selectively induce apoptosis of AML stem cells by disrupting lipid homeostasis, Cell Stem Cell (2021), https://doi.org/10.1016/j.stem.2021.06.004



suppression of SCD activity and consequent decrease in MUFAs contribute to the cytotoxicity of NAMPT inhibitors.

We hypothesized that the upregulation of SCD expression might serve as a protective response to counteract the decrease in MUFA:SFA ratio in NAD depleted cells. A prediction based on this hypothesis is that SCD inhibition should sensitize cells to NAMPT inhibitors. Indeed, treatment with two structurally distinct inhibitors of SCD, CAY10566 and MF-438, markedly sensitized THP-1 cells to KPT-9274 (Figures 5G and S5J). Next, we tested if activation of peroxisome proliferator-activated receptor gamma (PPARγ), a transcription factor that binds to the *SCD* promoter (Leung et al., 2019; Shinohara and Fujimori, 2020), would rescue THP-1 cells treated with KPT-9274. Treatment with troglitazone, a PPARγ agonist, upregulated *SCD* expression and rescued the viability of KPT-9274 treated cells (Figures 5H and S5K). This protective effect was neutralized by the addition of CAY10566 (Figure 5H), indicating that the effect was dependent on SCD activity. To study the role of SCD in primary samples, we measured *in vitro* sensitivity to KPT-9274 in the 11 primary AML samples that had previously been analyzed for SCD upregulation after drug treatment (Figure 5A). Consistent with our functional studies, SCD upregulation correlated with reduced drug sensitivity (Figure S5L). Our findings suggest that the induction of SREBP-regulated genes, and in particular *SCD*, is an adaptive protective response to NAD depletion, and suppression of this response may sensitize AML cells to NAMPT inhibitors.

## Dipyridamole potentiates ROS- and caspase-dependent cell death induced by KPT-9274

To explore the translational potential of our findings, we sought clinically approved drugs with inhibitory activity against SREBP signaling that could be repurposed to enhance the anti-leukemic activity of KPT-9274. Dipyridamole (DP) is a phosphodiesterase inhibitor with anti-platelet activity and is currently approved for secondary stroke prevention (Sacco et al., 2006). In addition to its anti-platelet properties, it has been shown to inhibit the activation of SREBPs and their target genes in multiple cancer types (Göbel et al., 2019; Longo et al., 2019, 2020; Pandyra et al., 2014; Zhou et al., 2020). Thus, we reasoned that treatment with DP should enhance the cytotoxicity of KPT-9274 through its inhibitory effects on SREBPs. Addition of DP at a non-toxic concentration sensitized THP-1 cells to the cytotoxic effects of KPT-9274 and FK-866 (Figures 6A and S6A). DP treatment blunted the induction of *HMGCR* expression in response to KPT-9274 (Figure S6B). A similar sensitization effect was observed in SIG-M5 AML cells, which are intrinsically resistant to KPT-9274 up to 500 nM (Figure 6A). This combination was also more effective in depleting the LSC-enriched $CD34^+CD38^-$ fraction of OCI-AML-8227 than either drug alone (Figure 6B).

To study the mechanism by which DP enhances sensitivity to KPT-9274, we performed a series of rescue experiments aimed at identifying the critical mediators of cell death. We first tested the impact of exogenous OA, as it effectively rescued cells from single agent KPT-9274 treatment (Figure 5F). Exogeneous OA also prevented cell death induced by the combination of DP and KPT-9274 (Figure 6C), implicating lipotoxicity as the cause of cell death. The mechanism by which lipotoxicity triggers cell death has been linked to the generation of mitochondrial superoxide and consequent oxidative damage to cellular components (Griffiths et al., 2013; Ly et al., 2017; Williams et al., 2013). To study the role of oxidative stress, we measured the effect of drug treatment on the level of mitochondrial superoxide, cytoplasmic ROS, and lipid ROS using compartment-specific and redox-sensitive fluorescent dyes. Treatment with single-agent KPT-9274 increased ROS levels in all three compartments that were further increased with the addition of DP in THP-1 cells (Figures 6D and S6C). KPT-9274 treatment also increased cytoplasmic and lipid ROS levels in OCI-AML-8227, with a greater increase observed in the $CD34^+$ fractions than in $CD34^-$ cells (Figure 6E). Exogenous OA attenuated the increase in ROS induced by KPT-9274 alone or in combination

**Figure 6. Dipyridamole potentiates ROS- and caspase-dependent cell death induced by KPT-9274**

(A) Percentage of dead THP-1 and SIG-M5 cells treated with DMSO or KPT-9274 in the presence or absence of DP at 10 μM for 48 h. DP was added 1 h prior to treatment with KPT-9274. n = 3 independent experiments.

(B) Number of viable $CD34^+CD38^-$ cells in OCI-AML-8227 treated with DMSO or KPT-9274 in the presence or absence of DP at 10 μM for 48 h. DP was added 1 h prior to treatment with KPT-9274. n = 3 independent experiments.

(C) Percentage of dead THP-1 cells treated with DMSO or KPT-9274 in the presence or absence of DP at 10 μM and OA at 75 μM for 48 h. DP and OA were added 1 h prior to treatment with KPT-9274. n = 3 independent experiments.

(D) Fold change in lipid ROS, cytoplasmic ROS, and mitochondrial superoxide levels in THP-1 cells treated with KPT-9274, DP at 10 μM, NAC at 10 mM, OA at 75 μM, or their combinations for 48 h. DP, NAC, and OA were added 1 h prior to treatment with KPT-9274. n = 3 independent experiments. *$p \leq 0.05$ compared with values for KPT-9274 at 30 nM plus DP. #$p \leq 0.05$ compared with values for KPT-9274 at 60 nM.

(E) Fold change in lipid ROS and cytoplasmic ROS in the indicated fractions of OCI-AML-8227 treated with KPT-9274 at 1.5 μM for 48 h relative to DMSO-treated cells. n = 3 independent experiments.

(F) Percentage of THP-1 cells with active caspase-3/7 treated with KPT-9274, DP (10 μM), NAC (10 mM), OA (75 μM) or their combinations for 48 h. DP, NAC, and OA were added 1 h prior to treatment with KPT-9274. n = 3 independent experiments.

(G) Percentage of dead THP-1 cells after treatment with KPT-9274, DP (10 μM), Z-VAD-FMK (50 μM), or their combinations for 48 h. DP and Z-VAD-FMK were added 1 h prior to treatment with KPT-9274. n = 3 independent experiments.

(H) Human engraftment in BM of primary NSG recipients transplanted with primary AML sample 130578 and treated with vehicle, KPT-9274 alone (150 mg/kg twice a day), DP alone (120 mg/kg per day), or KPT-9274 plus DP for 3 weeks on a 5-days-on, 2-day-off schedule. Engraftment was confirmed and quantified before starting treatment. Data shown are normalized to the pre-treatment engraftment level for each animal. Each data point represents an individual mouse. n = 5–7 mice per treatment arm.

(I) Human engraftment in the BM of secondary NSG recipients at 7 weeks after transplantation with an equal number of BM cells collected from animals shown in (H). Each data point represents an individual mouse. n = 8–9 mice per arm.

Data shown are mean ± SEM. Unless otherwise noted, statistical significance was determined using unpaired two-tailed Student's t test. *$p \leq 0.05$. See also Figure S6.

Please cite this article in press as: Subedi et al., Nicotinamide phosphoribosyltransferase inhibitors selectively induce apoptosis of AML stem cells by disrupting lipid homeostasis, Cell Stem Cell (2021), https://doi.org/10.1016/j.stem.2021.06.004





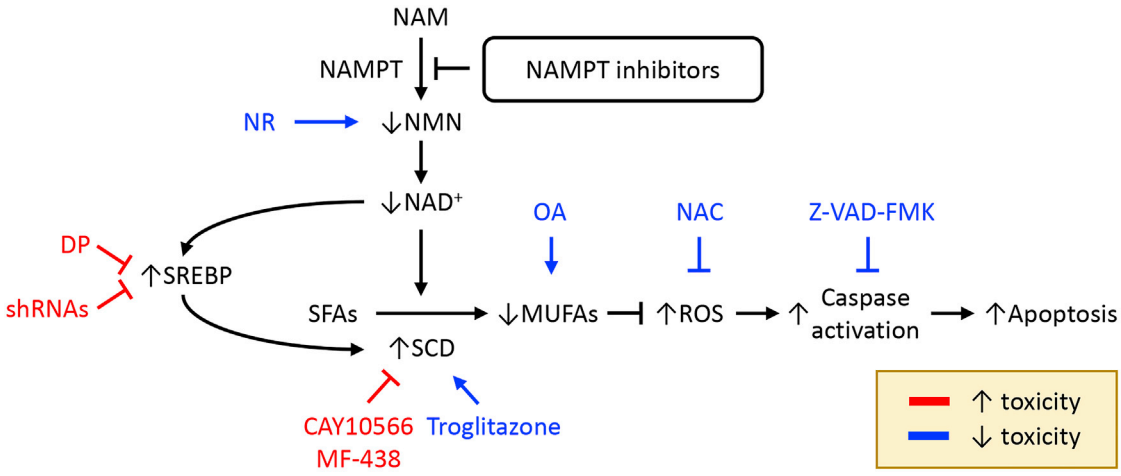


**Figure 7. Proposed mechanism by which NAMPT inhibition induces AML cell death through disruption of lipid homeostasis**
See text for details.

with DP in THP-1 cells (Figures 6D and S6C), suggesting that OA protects against their cytotoxic effects by reducing oxidative stress. In support of this notion, treatment with the antioxidant N-acetyl cysteine (NAC) lowered ROS levels (Figures 6D and S6C) and reduced cell death induced by KPT-9274 alone or in combination with DP (Figure S6D).

Lipotoxicity has previously been shown to be mediated through caspase-dependent apoptosis (Mota et al., 2016). Consistent with this mode of cell death, the levels of active caspase-3 and caspase-7 were increased in THP-1 cells treated with KPT-9274 and further enhanced with the addition of DP (Figure 6F), an effect that was abrogated by the addition of OA or NAC (Figure 6F). Furthermore, treatment with Z-VAD-FMK, a pan-caspase inhibitor, effectively suppressed cell death induced by KPT-9274 alone or in combination with DP (Figure 6G), indicating that caspase activation is required for cell death execution. Importantly, two inhibitors of ferroptosis, ferrostatin-1 and liproxstatin-1 (Dixon et al., 2012; Friedmann Angeli et al., 2014) failed to rescue the viability of cells treated with KPT-9274 (Figures S6E and S6F), arguing against ferroptosis as a major contributor of cell death. Taken together, our results indicate that the addition of DP to KPT-9274 enhances caspase-dependent apoptosis by exacerbating lipotoxicity and oxidative stress.

To determine if DP synergizes with KPT-9274 *in vivo*, we generated PDX models using AML sample 130578, which had previously failed to respond to single agent KPT-9274 treatment (Figures 3H and 3I). We transplanted cells from this sample into conditioned NSG mice and confirmed leukemic engraftment in BM at 6 weeks post-transplantation (Figure S6G). The engrafted mice were then randomized to receive treatment with vehicle, DP alone (120 mg/kg per day by intraperitoneal injection), KPT-9274 alone (150 mg/kg twice daily by oral administration), or DP plus KPT-9274 for 3 weeks on a 5-days-on, 2-days-off schedule. At the end of treatment, leukemic burden in BM was lowest in the combination treatment arm compared with the other arms (Figures 6H and S6H). To determine if LSCs were targeted, we harvested BM cells from primary recipients at the end of treatment, transplanted equivalent numbers of cells into secondary NSG recipients, and analyzed for human engraftment at 6 weeks post-transplantation. In contrast to the first series of *in vivo* experiments with sample 130578 (Figure 3I), KPT-9274 treatment alone was effective in reducing secondary engraftment potential (Figure 6I). Nevertheless, the addition of DP to KPT-9274 further reduced engraftment in secondary recipients (Figure 6I), demonstrating the superior efficacy of this drug combination in targeting LSCs *in vivo*.

## DISCUSSION

Our study demonstrates that AML stem cells are more dependent on the $NAD^+$ salvage pathway than normal HSPCs, resulting in a higher sensitivity to NAMPT inhibitors. Jones et al. (2020) reported similar findings in a recent study, but the reason for this differential dependency was not explored. Here, we showed that LSCs have less capacity to use the PH pathway to sustain $NAD^+$ generation upon NAMPT inhibition than normal HSPCs. The reduced capacity in LSCs is likely due to a lower level of NAPRT expression, which has been shown to be inversely correlated with sensitivity to NAMPT inhibitors across tumor types (Chowdhry et al., 2019). However, other mechanisms involving deficiencies in the uptake of NA and/or downstream enzymatic steps in the PH pathway cannot be excluded. Regardless of the precise mechanism, this finding suggests that NA supplementation may improve the therapeutic window of NAMPT inhibitors for AML treatment.

The cause of cancer cell death upon NAMPT inhibition has often been attributed to impairment of energy metabolism (Cagnetta et al., 2015; Jones et al., 2020; Mitchell et al., 2019). However, this mechanism has not been formally proved through rescue experiments. Here, we showed that disruption of lipid homeostasis is an important contributor to cell death in AML. On the basis of our findings, we propose a model in which depletion of intracellular $NAD^+$ levels by NAMPT inhibition compromises the desaturation activity of SCD, thereby disrupting the homeostatic balance between SFAs and MUFAs (Figure 7). This imbalance in turn causes lipotoxicity and triggers apoptosis in a ROS- and caspase-dependent manner (Figure 7).

Please cite this article in press as: Subedi et al., Nicotinamide phosphoribosyltransferase inhibitors selectively induce apoptosis of AML stem cells by disrupting lipid homeostasis, Cell Stem Cell (2021), https://doi.org/10.1016/j.stem.2021.06.004



Lipotoxicity, generally defined as the accumulation of excess lipid, has long been recognized as a cause of cell dysfunction and cell death in non-adipose tissues (Brookheart et al., 2009). However, not all lipid species are equally cytotoxic, with SFAs showing a strong cytotoxic effect, whereas unsaturated FAs are generally non-toxic and can prevent the toxicity of SFAs (de Vries et al., 1997; Listenberger et al., 2003; Maedler et al., 2003). The mechanism by which lipotoxicity causes apoptotic cell death has been shown to be mediated, at least in part, through increased mitochondrial superoxide overproduction and consequent oxidative stress (Lee et al., 2017a, 2017b). Consistent with this mechanism, we found that replenishing the MUFA pool with exogenous OA reduced the high levels of ROS and cell death induced by KPT-9274. These findings highlight the importance of lipotoxicity as a cause of death in AML cells upon NAMPT inhibition.

SREBPs are key transcriptional regulators of genes involved in lipid homeostasis. Our transcriptomic analysis revealed a robust upregulation of known SREBP target genes upon KPT-9274 treatment. As deficiency of unsaturated FAs has been shown to increase the expression and processing of SREBPs (Hannah et al., 2001; Worgall et al., 1998), we postulate that the SREBP transcriptional response is a homeostatic reaction to depletion of MUFAs. Indeed, an important role of SREBP signaling is to promote SCD-mediated desaturation, thereby normalizing the MUFA/SFA ratio and protecting cancer cells from lipotoxicity (Williams et al., 2013; Zhang et al., 2019b). Consistent with these studies, we showed that inhibition of either SREBP2 or SCD sensitized AML cells to NAMPT inhibition, indicating that the SREBP-SCD axis is protective against NAD depletion. Mechanistic insights gained from our study support the co-administration of SREBP inhibitors to enhance the therapeutic efficacy of NAMPT inhibitors. DP is a particularly attractive combination partner given its excellent safety track record as an anti-platelet agent and demonstrated ability to block SREBP activation (Göbel et al., 2019; Longo et al., 2019, 2020; Pandyra et al., 2014; Zhou et al., 2020).

Despite recent advances, AML remains a challenging disease to treat and frequently relapses after achieving initial remission with conventional induction chemotherapy or lower intensity regimens. The addition of NAMPT inhibitors to these existing therapies may delay or prevent disease relapse by enhancing the depletion of LSCs. Our findings corroborate those of a previous study showing that LSCs from relapsed/refractory (R/R) samples are sensitive to NAMPT inhibition (Jones et al., 2020). However, in contrast to that study, we found that LSCs from diagnostic untreated samples are also sensitive to NAMPT inhibitors, suggesting that NAMPT inhibitors are effective not only for R/R patients but also treatment-naive patients. In addition, we propose that NAMPT inhibitors could be used as maintenance therapy for patients at high risk for relapse and should be administered in combination with SREBP inhibitors and/or other LSC-targeting agents, such as venetoclax (Mitchell et al., 2019; Pollyea et al., 2018), to maximize their anti-LSC activity.

### Limitations of the study

There are several limitations to our study that should be taken into consideration. First, most of our experiments were done using pharmacologic manipulations, which could have potential off-target effects. To address this issue, we performed rescue experiments and used several structurally unrelated compounds to demonstrate target specificity. Nevertheless, potential off-target effects are possible with drugs such as troglitazone, which has pleiotropic effects beyond its role in increasing *SCD* expression. Second, our RNA-seq analysis revealed changes in expression of genes that are not related to the SREBP-regulated response, suggesting that other mechanisms might contribute to the effects of KPT-9274. Similarly, we observed substantial changes in the levels of many metabolites that are not directly involved with lipid metabolism, including intermediates in the TCA cycle (e.g., 2-oxoglutarate and citrate) and glycolysis (e.g., fructose 1,6-bisphosphate and glucose 6-phosphate). These widespread changes are consistent with the central role of $NAD^+$ in metabolism and thus, alternative mechanisms may contribute to the cellular effects of $NAD^+$ depletion. Last, it is unclear if there are subtypes of AML that are more or less responsive to NAMPT inhibition. We showed that SCD upregulation is a potential biomarker of resistance, but this finding needs to be validated using a larger number of AML samples.

## STAR★METHODS

Detailed methods are provided in the online version of this paper and include the following:

- KEY RESOURCES TABLE
- RESOURCE AVAILABILITY
  - Lead contact
  - Materials availability
  - Data and code availability
- EXPERIMENTAL MODEL AND SUBJECT DETAILS
  - Human cell lines
  - Primary AML cells and cord blood HSPCs
  - Mouse studies
- METHOD DETAILS
  - Primary and secondary drug screen
  - Determination of LSC gene signature
  - NSG xenotransplantation
  - *In vivo* drug treatments
  - Bone marrow engraftment analysis
  - Bioluminescence imaging
  - Cell viability assessment
  - Cell cycle analysis
  - Colony forming unit assay
  - Western blot
  - Intracellular staining for NAMPT expression
  - NAD quantification by LC/MS
  - NAD quantification by colorimetric kit
  - NAD quantification after *in vivo* treatment
  - Metabolomic analysis
  - Lentiviral vectors encoding shRNAs
  - Lentiviral production and AML transduction
  - RNA sequencing
  - Real-time quantitative PCR (qPCR)
  - Reactive oxygen species measurements
  - Active caspase 3/7 assay
- QUANTIFICATION AND STATISTICAL ANALYSIS

## SUPPLEMENTAL INFORMATION

Supplemental information can be found online at https://doi.org/10.1016/j.stem.2021.06.004.

## ACKNOWLEDGMENTS

We acknowledge support from the Princess Margaret Leukemia Tissue Bank and the patients who donated samples used in this study. This project was supported by the Acute Leukemia Translational Research Initiative from the Ontario Institute for Cancer Research. S.M.C. is generously supported by the Princess Margaret Cancer Foundation, a Leukemia Research Foundation New Investigator Award, and Canadian Institutes of Health Research (CIHR) grants PJT-159521 and PJT-175186. We also wish to thank the SPARC Bio-Centre at the Hospital for Sick Children and OICR Drug Discovery Program for their support with drug screening.

## AUTHOR CONTRIBUTIONS

A.S. and S.M.C. wrote the manuscript. A.S., Q.L., J.C.Y.W., and S.M.C. designed the study and analyzed results. A.S., Q.L., D.M.A., D.S., S.C., M.H., and E.R.L. performed the experiments. C.X., V.V., and G.D.B. performed the bioinformatic analysis of drug screen. A.D. performed the metabolomic analysis. M.D.M. and J.E.D. supervised research. J.C.Y.W. and S.M.C. provided funding and study supervision. All authors reviewed the manuscript.

## DECLARATION OF INTERESTS

The authors declare no competing interests.

Received: September 28, 2020
Revised: May 5, 2021
Accepted: June 22, 2021
Published: July 21, 2021

## REFERENCES

Abu Aboud, O., Chen, C.H., Senapedis, W., Baloglu, E., Argueta, C., and Weiss, R.H. (2016). Dual and specific inhibition of NAMPT and PAK4 by KPT-9274 decreases kidney cancer growth. Mol. Cancer Ther. *15*, 2119–2129.

Biddle, A., Gammon, L., Liang, X., Costea, D.E., and Mackenzie, I.C. (2016). Phenotypic plasticity determines cancer stem cell therapeutic resistance in oral squamous cell carcinoma. EBioMedicine *4*, 138–145.

Bonnet, D., and Dick, J.E. (1997). Human acute myeloid leukemia is organized as a hierarchy that originates from a primitive hematopoietic cell. Nat. Med. *3*, 730–737.

Brookheart, R.T., Michel, C.I., and Schaffer, J.E. (2009). As a matter of fat. Cell Metab. *10*, 9–12.

Cagnetta, A., Caffa, I., Acharya, C., Soncini, D., Acharya, P., Adamia, S., Pierri, I., Bergamaschi, M., Garuti, A., Fraternali, G., et al. (2015). APO866 increases antitumor activity of cyclosporin-A by inducing mitochondrial and endoplasmic reticulum stress in leukemia cells. Clin. Cancer Res. *21*, 3934–3945.

Chan, S.M., Thomas, D., Corces-Zimmerman, M.R., Xavy, S., Rastogi, S., Hong, W.J., Zhao, F., Medeiros, B.C., Tyvoll, D.A., and Majeti, R. (2015). Isocitrate dehydrogenase 1 and 2 mutations induce BCL-2 dependence in acute myeloid leukemia. Nat. Med. *21*, 178–184.

Chowdhry, S., Zanca, C., Rajkumar, U., Koga, T., Diao, Y., Raviram, R., Liu, F., Turner, K., Yang, H., Brunk, E., et al. (2019). NAD metabolic dependency in cancer is shaped by gene amplification and enhancer remodelling. Nature *569*, 570–575.

de Vries, J.E., Vork, M.M., Roemen, T.H., de Jong, Y.F., Cleutjens, J.P., van der Vusse, G.J., and van Bilsen, M. (1997). Saturated but not mono-unsaturated fatty acids induce apoptotic cell death in neonatal rat ventricular myocytes. J. Lipid Res. *38*, 1384–1394.

Dixon, S.J., Lemberg, K.M., Lamprecht, M.R., Skouta, R., Zaitsev, E.M., Gleason, C.E., Patel, D.N., Bauer, A.J., Cantley, A.M., Yang, W.S., et al. (2012). Ferroptosis: an iron-dependent form of nonapoptotic cell death. Cell *149*, 1060–1072.

Dombret, H., and Gardin, C. (2016). An update of current treatments for adult acute myeloid leukemia. Blood *127*, 53–61.

Friedmann Angeli, J.P., Schneider, M., Proneth, B., Tyurina, Y.Y., Tyurin, V.A., Hammond, V.J., Herbach, N., Aichler, M., Walch, A., Eggenhofer, E., et al. (2014). Inactivation of the ferroptosis regulator Gpx4 triggers acute renal failure in mice. Nat. Cell Biol. *16*, 1180–1191.

Galli, U., Colombo, G., Travelli, C., Tron, G.C., Genazzani, A.A., and Grolla, A.A. (2020). Recent advances in NAMPT inhibitors: a novel immunotherapic strategy. Front. Pharmacol. *11*, 656.

Gehrke, S., Rice, S., Stefanoni, D., Wilkerson, R.B., Nemkov, T., Reisz, J.A., Hansen, K.C., Lucas, A., Cabrales, P., Drew, K., and D'Alessandro, A. (2019). Red blood cell metabolic responses to torpor and arousal in the hibernator arctic ground squirrel. J. Proteome Res. *18*, 1827–1841.

Göbel, A., Breining, D., Rauner, M., Hofbauer, L.C., and Rachner, T.D. (2019). Induction of 3-hydroxy-3-methylglutaryl-CoA reductase mediates statin resistance in breast cancer cells. Cell Death Dis. *10*, 91.

Griffiths, B., Lewis, C.A., Bensaad, K., Ros, S., Zhang, Q., Ferber, E.C., Konisti, S., Peck, B., Miess, H., East, P., et al. (2013). Sterol regulatory element binding protein-dependent regulation of lipid synthesis supports cell survival and tumor growth. Cancer Metab. *1*, 3.

Guzman, M.L., Rossi, R.M., Karnischky, L., Li, X., Peterson, D.R., Howard, D.S., and Jordan, C.T. (2005). The sesquiterpene lactone parthenolide induces apoptosis of human acute myelogenous leukemia stem and progenitor cells. Blood *105*, 4163–4169.

Hannah, V.C., Ou, J., Luong, A., Goldstein, J.L., and Brown, M.S. (2001). Unsaturated fatty acids down-regulate srebp isoforms 1a and 1c by two mechanisms in HEK-293 cells. J. Biol. Chem. *276*, 4365–4372.

Horton, J.D., Goldstein, J.L., and Brown, M.S. (2002). SREBPs: activators of the complete program of cholesterol and fatty acid synthesis in the liver. J. Clin. Invest. *109*, 1125–1131.

Horton, J.D., Shah, N.A., Warrington, J.A., Anderson, N.N., Park, S.W., Brown, M.S., and Goldstein, J.L. (2003). Combined analysis of oligonucleotide microarray data from transgenic and knockout mice identifies direct SREBP target genes. Proc. Natl. Acad. Sci. U S A *100*, 12027–12032.

Ito, K., and Suda, T. (2014). Metabolic requirements for the maintenance of self-renewing stem cells. Nat. Rev. Mol. Cell Biol. *15*, 243–256.

Jones, C.L., Stevens, B.M., D'Alessandro, A., Reisz, J.A., Culp-Hill, R., Nemkov, T., Pei, S., Khan, N., Adane, B., Ye, H., et al. (2018). Inhibition of amino acid metabolism selectively targets human leukemia stem cells. Cancer Cell *34*, 724–740.e4.

Jones, C.L., Stevens, B.M., Pollyea, D.A., Culp-Hill, R., Reisz, J.A., Nemkov, T., Gehrke, S., Gamboni, F., Krug, A., Winters, A., et al. (2020). Nicotinamide metabolism mediates resistance to venetoclax in relapsed acute myeloid leukemia stem cells. Cell Stem Cell *27*, 748–764.e4.

Kaufmann, K.B., Garcia-Prat, L., Liu, Q., Ng, S.W.K., Takayanagi, S.I., Mitchell, A., Wienholds, E., van Galen, P., Cumbaa, C.A., Tsay, M.J., et al. (2019). A stemness screen reveals *C3orf54/INKA1* as a promoter of human leukemia stem cell latency. Blood *133*, 2198–2211.

Kozako, T., Aikawa, A., Ohsugi, T., Uchida, Y.I., Kato, N., Sato, K., Ishitsuka, K., Yoshimitsu, M., and Honda, S.I. (2019). High expression of NAMPT in adult T-cell leukemia/lymphoma and anti-tumor activity of a NAMPT inhibitor. Eur. J. Pharmacol. *865*, 172738.

Lagadinou, E.D., Sach, A., Callahan, K., Rossi, R.M., Neering, S.J., Minhajuddin, M., Ashton, J.M., Pei, S., Grose, V., O'Dwyer, K.M., et al. (2013). BCL-2 inhibition targets oxidative phosphorylation and selectively eradicates quiescent human leukemia stem cells. Cell Stem Cell *12*, 329–341.

Lechman, E.R., Gentner, B., Ng, S.W.K., Schoof, E.M., van Galen, P., Kennedy, J.A., Nucera, S., Ciceri, F., Kaufmann, K.B., Takayama, N., et al.

(2016). miR-126 regulates distinct self-renewal outcomes in normal and malignant hematopoietic stem cells. Cancer Cell *29*, 602–606.

Lee, E.A., Angka, L., Rota, S.G., Hanlon, T., Mitchell, A., Hurren, R., Wang, X.M., Gronda, M., Boyaci, E., Bojko, B., et al. (2015). Targeting mitochondria with avocatin B induces selective leukemia cell death. Cancer Res. *75*, 2478–2488.

Lee, E., Choi, J., and Lee, H.S. (2017a). Palmitate induces mitochondrial superoxide generation and activates AMPK in podocytes. J. Cell. Physiol. *232*, 3209–3217.

Lee, H., Lim, J.Y., and Choi, S.J. (2017b). Oleate prevents palmitate-induced atrophy via modulation of mitochondrial ROS production in skeletal myotubes. Oxid. Med. Cell. Longev. *2017*, 2739721.

Leung, D.T.H., Rainczuk, A., Nguyen, T., Stephens, A., Silke, J., Fuller, P.J., and Chu, S. (2019). Targeting XIAP and PPARγ in granulosa cell tumors alters metabolic signaling. J. Proteome Res. *18*, 1691–1702.

Listenberger, L.L., Han, X., Lewis, S.E., Cases, S., Farese, R.V., Jr., Ory, D.S., and Schaffer, J.E. (2003). Triglyceride accumulation protects against fatty acid-induced lipotoxicity. Proc. Natl. Acad. Sci. U S A *100*, 3077–3082.

Longo, J., Mullen, P.J., Yu, R., van Leeuwen, J.E., Masoomian, M., Woon, D.T.S., Wang, Y., Chen, E.X., Hamilton, R.J., Sweet, J.M., et al. (2019). An actionable sterol-regulated feedback loop modulates statin sensitivity in prostate cancer. Mol. Metab. *25*, 119–130.

Longo, J., Pandyra, A.A., Stachura, P., Minden, M.D., Schimmer, A.D., and Penn, L.Z. (2020). Cyclic AMP-hydrolyzing phosphodiesterase inhibitors potentiate statin-induced cancer cell death. Mol. Oncol. *14*, 2533–2545.

Ly, L.D., Xu, S., Choi, S.K., Ha, C.M., Thoudam, T., Cha, S.K., Wiederkehr, A., Wollheim, C.B., Lee, I.K., and Park, K.S. (2017). Oxidative stress and calcium dysregulation by palmitate in type 2 diabetes. Exp. Mol. Med. *49*, e291.

Maedler, K., Oberholzer, J., Bucher, P., Spinas, G.A., and Donath, M.Y. (2003). Monounsaturated fatty acids prevent the deleterious effects of palmitate and high glucose on human pancreatic beta-cell turnover and function. Diabetes *52*, 726–733.

Matsumoto, T., Uchiumi, T., Monji, K., Yagi, M., Setoyama, D., Amamoto, R., Matsushima, Y., Shiota, M., Eto, M., and Kang, D. (2017). Doxycycline induces apoptosis via ER stress selectively to cells with a cancer stem cell-like properties: importance of stem cell plasticity. Oncogenesis *6*, 397.

Mitchell, S.R., Larkin, K., Grieselhuber, N.R., Lai, T.H., Cannon, M., Orwick, S., Sharma, P., Asemelash, Y., Zhang, P., Goettl, V.M., et al. (2019). Selective targeting of NAMPT by KPT-9274 in acute myeloid leukemia. Blood Adv. *3*, 242–255.

Molina, J.R., Sun, Y., Protopopova, M., Gera, S., Bandi, M., Bristow, C., McAfoos, T., Morlacchi, P., Ackroyd, J., Agip, A.A., et al. (2018). An inhibitor of oxidative phosphorylation exploits cancer vulnerability. Nat. Med. *24*, 1036–1046.

Mota, M., Banini, B.A., Cazanave, S.C., and Sanyal, A.J. (2016). Molecular mechanisms of lipotoxicity and glucotoxicity in nonalcoholic fatty liver disease. Metabolism *65*, 1049–1061.

Nacarelli, T., Fukumoto, T., Zundell, J.A., Fatkhutdinov, N., Jean, S., Cadungog, M.G., Borowsky, M.E., and Zhang, R. (2020). NAMPT inhibition suppresses cancer stem-like cells associated with therapy-induced senescence in ovarian cancer. Cancer Res. *80*, 890–900.

Nemkov, T., Hansen, K.C., and D'Alessandro, A. (2017). A three-minute method for high-throughput quantitative metabolomics and quantitative tracing experiments of central carbon and nitrogen pathways. Rapid Commun. Mass Spectrom. *31*, 663–673.

Nemkov, T., Reisz, J.A., Gehrke, S., Hansen, K.C., and D'Alessandro, A. (2019). High-throughput metabolomics: isocratic and gradient mass spectrometry-based methods. Methods Mol. Biol. *1978*, 13–26.

Ng, S.W., Mitchell, A., Kennedy, J.A., Chen, W.C., McLeod, J., Ibrahimova, N., Arruda, A., Popescu, A., Gupta, V., Schimmer, A.D., et al. (2016). A 17-gene stemness score for rapid determination of risk in acute leukaemia. Nature *540*, 433–437.

Ogino, Y., Sato, A., Uchiumi, F., and Tanuma, S.I. (2018). Cross resistance to diverse anticancer nicotinamide phosphoribosyltransferase inhibitors induced by FK866 treatment. Oncotarget *9*, 16451–16461.

Pandyra, A., Mullen, P.J., Kalkat, M., Yu, R., Pong, J.T., Li, Z., Trudel, S., Lang, K.S., Minden, M.D., Schimmer, A.D., and Penn, L.Z. (2014). Immediate utility of two approved agents to target both the metabolic mevalonate pathway and its restorative feedback loop. Cancer Res. *74*, 4772–4782.

Pollyea, D.A., Stevens, B.M., Jones, C.L., Winters, A., Pei, S., Minhajuddin, M., D'Alessandro, A., Culp-Hill, R., Riemondy, K.A., Gillen, A.E., et al. (2018). Venetoclax with azacitidine disrupts energy metabolism and targets leukemia stem cells in patients with acute myeloid leukemia. Nat. Med. *24*, 1859–1866.

Sacco, R.L., Adams, R., Albers, G., Alberts, M.J., Benavente, O., Furie, K., Goldstein, L.B., Gorelick, P., Halperin, J., Harbaugh, R., et al.; American Heart Association; American Stroke Association Council on Stroke; Council on Cardiovascular Radiology and Intervention; American Academy of Neurology (2006). Guidelines for prevention of stroke in patients with ischemic stroke or transient ischemic attack: a statement for healthcare professionals from the American Heart Association/American Stroke Association Council on Stroke: co-sponsored by the Council on Cardiovascular Radiology and Intervention: the American Academy of Neurology affirms the value of this guideline. Stroke *37*, 577–617.

Sharon, D., Cathelin, S., Mirali, S., Di Trani, J.M., Yanofsky, D.J., Keon, K.A., Rubinstein, J.L., Schimmer, A.D., Ketela, T., and Chan, S.M. (2019). Inhibition of mitochondrial translation overcomes venetoclax resistance in AML through activation of the integrated stress response. Sci. Transl. Med. *11*, eaax2863.

Shinohara, S., and Fujimori, K. (2020). Promotion of lipogenesis by PPARγ-activated FXR expression in adipocytes. Biochem. Biophys. Res. Commun. *527*, 49–55.

Shlush, L.I., Mitchell, A., Heisler, L., Abelson, S., Ng, S.W.K., Trotman-Grant, A., Medeiros, J.J.F., Rao-Bhatia, A., Jaciw-Zurakowsky, I., Marke, R., et al. (2017). Tracing the origins of relapse in acute myeloid leukaemia to stem cells. Nature *547*, 104–108.

Skrtić, M., Sriskanthadevan, S., Jhas, B., Gebbia, M., Wang, X., Wang, Z., Hurren, R., Jitkova, Y., Gronda, M., Maclean, N., et al. (2011). Inhibition of mitochondrial translation as a therapeutic strategy for human acute myeloid leukemia. Cancer Cell *20*, 674–688.

Viale, A., Pettazzoni, P., Lyssiotis, C.A., Ying, H., Sánchez, N., Marchesini, M., Carugo, A., Green, T., Seth, S., Giuliani, V., et al. (2014). Oncogene ablation-resistant pancreatic cancer cells depend on mitochondrial function. Nature *514*, 628–632.

Wang, Y., Liu, Y., Malek, S.N., Zheng, P., and Liu, Y. (2011). Targeting HIF1α eliminates cancer stem cells in hematological malignancies. Cell Stem Cell *8*, 399–411.

Williams, K.J., Argus, J.P., Zhu, Y., Wilks, M.Q., Marbois, B.N., York, A.G., Kidani, Y., Pourzia, A.L., Akhavan, D., Lisiero, D.N., et al. (2013). An essential requirement for the SCAP/SREBP signaling axis to protect cancer cells from lipotoxicity. Cancer Res. *73*, 2850–2862.

Worgall, T.S., Sturley, S.L., Seo, T., Osborne, T.F., and Deckelbaum, R.J. (1998). Polyunsaturated fatty acids decrease expression of promoters with sterol regulatory elements by decreasing levels of mature sterol regulatory element-binding protein. J. Biol. Chem. *273*, 25537–25540.

Young, R.M., Ackerman, D., Quinn, Z.L., Mancuso, A., Gruber, M., Liu, L., Giannoukos, D.N., Bobrovnikova-Marjon, E., Diehl, J.A., Keith, B., and Simon, M.C. (2013). Dysregulated mTORC1 renders cells critically dependent on desaturated lipids for survival under tumor-like stress. Genes Dev. *27*, 1115–1131.

Zhang, L.Y., Liu, L.Y., Qie, L.L., Ling, K.N., Xu, L.H., Wang, F., Fang, S.H., Lu, Y.B., Hu, H., Wei, E.Q., and Zhang, W.P. (2012). Anti-proliferation effect of APO866 on C6 glioblastoma cells by inhibiting nicotinamide phosphoribosyltransferase. Eur. J. Pharmacol. *674*, 163–170.

Zhang, C., Tong, J., and Huang, G. (2013). Nicotinamide phosphoribosyl transferase (Nampt) is a target of microRNA-26b in colorectal cancer cells. PLoS ONE *8*, e69963.

Zhang, H., Zhang, N., Liu, Y., Su, P., Liang, Y., Li, Y., Wang, X., Chen, T., Song, X., Sang, Y., et al. (2019a). Epigenetic regulation of *NAMPT* by *NAMPT-AS* drives metastatic progression in triple-negative breast cancer. Cancer Res. *79*, 3347–3359.

Zhang, Y., Li, C., Hu, C., Wu, Q., Cai, Y., Xing, S., Lu, H., Wang, L., Huang, D., Sun, L., et al. (2019b). Lin28 enhances de novo fatty acid synthesis to promote cancer progression via SREBP-1. EMBO Rep. *20*, e48115.

Zhou, S., Xu, H., Tang, Q., Xia, H., and Bi, F. (2020). Dipyridamole enhances the cytotoxicities of trametinib against colon cancer cells through combined targeting of HMGCS1 and MEK pathway. Mol. Cancer Ther. *19*, 135–146.

Please cite this article in press as: Subedi et al., Nicotinamide phosphoribosyltransferase inhibitors selectively induce apoptosis of AML stem cells by disrupting lipid homeostasis, Cell Stem Cell (2021), https://doi.org/10.1016/j.stem.2021.06.004



## STAR★METHODS

### KEY RESOURCES TABLE

| REAGENT or RESOURCE | SOURCE | IDENTIFIER |
|---|---|---|
| **Antibodies** | | |
| CD34-APC | BD Biosciences | Cat# 340441; RRID:AB_400514 |
| CD38-PE | BD Biosciences | Cat# 12-0388-42; RRID:AB_1518748 |
| CD38-APC-R700 | BD Biosciences | Cat# 564980; RRID:AB_2744373 |
| CD14-PE | BD Biosciences | Cat# 562691; RRID:AB_2737725 |
| CD14-V450 | BD Biosciences | Cat# 560349; RRID:AB_1645559 |
| FcR blocking reagent | Miltenyi Biotech | Cat# 130-059-901 |
| Annexin V-FITC | BD Biosciences | Cat# 556419; RRID:AB_2665412 |
| Annexin V-FITC | Biolegend | Cat# 640905 |
| Annexin V-Alexa 647 | Thermo Fisher | Cat# A23204; RRID:AB_2341149 |
| Propidium iodide | Thermo Fisher Scientific | Cat# P1304MP |
| CD45.1-PeCy7 | Biolegend | Cat#110729; RRID:AB_1134168 |
| CD45-APC | Biolegend | Cat# 304037; RRID:AB_2562049 |
| IgG2A-Alexa Fluor 488 | R&D Systems | Cat# IC006G |
| Human/Mouse PBEF/Visfatin-Alexa Fluor 488 | R&D Systems | Cat# IC4044G |
| β-actin | Cell Signaling Technology | Cat# 3700; RRID:AB_2242334 |
| NAMPT (D1K6D) Rabbit mAb antibody | Cell Signaling Technology | Cat# 61122; RRID:AB_2799602 |
| Anti-NAPRT antibody | Abcam | Cat# ab211529 |
| SREBP-2 antibody | BD Biosciences | Cat# 557037; RRID:AB_396560 |
| SREBP-1 antibody | Abcam | Cat# ab3259; RRID:AB_303650 |
| Acetyl CoA synthetase antibody | Abcam | Cat# ab66038; RRID:AB_ 1859836 |
| Anti-HMGCR antibody [EPR1685(N)] | Abcam | Cat# ab174830; RRID:AB_ 2749818 |
| HMGCS1 (D5W8F) Rabbit mAb antibody | Cell Signaling Technology | Cat# 36877; RRID:AB_ 2799107 |
| SCD1 (C12H5) Rabbit mAb antibody | Cell Signaling Technology | Cat# 2794; RRID:AB_ 2183099 |
| IRDye 680LT goat anti-mouse | LI-COR Biosciences | Cat# 926-68020; RRID:AB_10706161 |
| IRDye 800CW goat anti-rabbit | LI-COR BioSciences | Cat# 926-32211; RRID:AB_621843 |
| **Biological samples** | | |
| Human cord blood | Trillium and Credit Valley Hospital | N/A |
| Primary AML samples | UHN biobank | N/A |
| **Chemicals, peptides, and recombinant proteins** | | |
| EasySep Human Progenitor Cell Enrichment Kit | Stem Cell Technologies | Cat# 19356 |
| EasySep Human CD3 Positive Selection Kit II | Stem Cell Technologies | Cat# 17851 |
| EasySep Mouse/Human Chimera Isolation Kit | Stem Cell Technologies | Cat# 19849 |
| MethoCult H4435 Enriched | Stem Cell Technologies | Cat# 04435 |
| RPMI 1640 | Wisent Bioproducts | Cat# 350-035-CL |
| DMEM | Wisent Bioproducts | Cat# 319-005-CL |
| Optim-MEM I | Thermo Fisher Scientific | Cat# 31985070 |
| Fetal bovine serum (FBS), | Wisent Bioproducts | Cat# 080-150 |
| Hanks balanced salt solution (HBSS) | Wisent Bioproducts | Cat# 311-513-CL |
| HBSS | Thermo Fisher Scientific | Cat# 14170-112 |
| Annexin Binding Buffer | Biolegend | Cat# 422201 |

(*Continued on next page*)

Please cite this article in press as: Subedi et al., Nicotinamide phosphoribosyltransferase inhibitors selectively induce apoptosis of AML stem cells by disrupting lipid homeostasis, Cell Stem Cell (2021), https://doi.org/10.1016/j.stem.2021.06.004





*Continued*

| REAGENT or RESOURCE | SOURCE | IDENTIFIER |
|---|---|---|
| CountBright Plus Absolute Counting Beads | Thermo Fisher Scientific | Cat# C36995 |
| HEPES | Thermo Fisher Scientific | Cat# 15630-080 |
| BSA | Wisent Bioproducts | Cat# 800-096-EG |
| Retronectin | Takara Bio | Cat# T100B |
| Sodium azide | Sigma | Cat# S2002-100G |
| Gluta-Plus | Wisent Bioproducts | Cat # 609-066-EL |
| Sodium pyruvate | Wisent Bioproducts | Cat # 600-110-EL |
| X-Vivo 10 | Lonza | Cat # 04-380Q |
| BIT 9500 | Stem Cell Technologies | Cat# 09500 |
| Dipyridamole | UHN Pharmacy | N/A |
| PEG 600 | Sigma | Cat# 8170045000 |
| Tartaric acid | Sigma | Cat# BM0025 |
| RBC Lysis Buffer | Biolegend | Cat# 420301 |
| Luciferin | PerkinElmer | Cat# 122799 |
| 7-AAD | BD Biosciences | Cat# 559925 |
| Fixation buffer | Biolegend | Cat# 420801 |
| Fixation/Permeabilization Solution Kit | BD Biosciences | Cat# 554714 |
| RIPA buffer | Sigma | Cat# R0278 |
| RNase A | Gold Biotechnology | Cat# R-050-50 |
| Halt Protease Inhibitor cocktail | Thermo Fisher Scientific | Cat# 87786 |
| Pierce BCA Protein Assay Kit | Thermo Fisher Scientific | Cat# 23227 |
| LDS sample buffer | Thermo Fisher Scientific | Cat# B0008 |
| Bolt™ 4 to 12% Bis-Tris gel | Thermo Fisher Scientific | Cat# NW04125BOX |
| Nitrocellulose membrane | Thermo Fisher Scientific | Cat# IB23001 |
| 293Fectin transfection reagent | Thermo Fisher Scientific | Cat# 12347-019 |
| PES filter | Thermo Fisher Scientific | Cat# 564-0020 |
| PEG 8000 | Sigma | Cat# 89510-1KG-F |
| Rneasy Plus Mini Kit | QIAGEN | Cat# 74136 |
| iScript Advanced cDNA Synthesis Kit | Bio-Rad | Cat# 1725038 |
| ADVANCED qPCR mastermix | Wisent Bioproducts | Cat# 800-435-UL |
| IL-6 | Peprotech | Cat# 200-06 |
| IL-3 | Peprotech | Cat# 200-03 |
| SCF | Peprotech | Cat# 300-07 |
| FLT3L | Peprotech | Cat # 300-19 |
| G-CSF | Peprotech | Cat# 300-23 |
| TPO | Peprotech | Cat# 300-18 |
| FK-866 | Sigma | Cat# F8557 |
| KPT-9274 | Karyopharam | N/A |
| GMX-1778 | Sigma | Cat# SML0646 |
| Simvastatin | Cayman Chemicals | Cat# 10010344 |
| Oleic acid | Cayman Chemicals | Cat# 90260 |
| Nicotinic acid | Sigma | Cat# N0761-100G |
| Nicotinamide riboside | Cayman Chemicals | Cat# 23132-1 |
| Farnesyl pyrophosphate | Sigma | Cat# F6892-1VL |
| Geranylgeranyl pyrophosphate | Sigma | Cat# G6025-1VL |
| Isopentenyl pyrophosphate | Sigma | Cat# I0503-1VL |
| Cholesterol–methyl-β-cyclodextrin | Sigma | Cat# C4951 |
| Mevalonolactone | Cayman Chemicals | Cat# 20348 |
| Palmitic acid | Sigma | Cat# P5585 |
| Dipyridamole | Cayman Chemicals | Cat# 18189 |

(*Continued on next page*)

*Continued*

| REAGENT or RESOURCE | SOURCE | IDENTIFIER |
|---|---|---|
| Troglitazone | Cayman Chemicals | Cat# 71750 |
| CAY10566 | Cayman Chemicals | Cat# 10012562 |
| MF-438 | Sigma | Cat# 569406 |
| NAC | Sigma | Cat# A9165 |
| RSL3 | Cayman Chemicals | Cat# 19288 |
| Ferrostatin-1 | Selleckchem | Cat# S7243 |
| Liproxstatin-1 | Cayman Chemicals | Cat# 17730 |
| Tet-inducible pRSITEP-U6Tet-(sh)-EF1-TetRep-2A-GFP lentiviral vector | Cellecta | Cat# SVSHU6TEP-L |
| **Critical commercial assays** | | |
| MycoAlert Mycoplasma Detection Kit | Lonza | Cat# LT07-318 |
| NAD/NADH Quantitation Colorimetric Kit | Biovision | Cat# K337 |
| C11 BODIPY 581/591 | Cayman Chemicals | Cat# 27086 |
| CellROX™ Deep Red | Thermo Fisher Scientific | Cat# C10422 |
| MitoSOX™ Red | Thermo Fisher | Cat# M36008 |
| FAM-FLICA Caspase 3/7 Assay kit | Bio-Rad | Cat# ICT093 |
| **Experimental models: Organisms/strains** | | |
| NOD/SCID/IL2rg−/− (NSG | The Jackson Laboratory | RRID:IMSR_JAX:005557 |
| **Oligonucleotides** | | |
| Primer Sequences | Tables S4 and S5 | N/A |
| **Deposited data** | | |
| Processed RNA-seq (FKPM) data in Figure 4 | Mendeley Data Site | https://doi.org/10.17632/r6z8xwd945.1 |
| **Software and algorithms** | | |
| FlowJo V10.7.1 | https://www.flowjo.com/solutions/flowjo | RRID:SCR_008520 |
| R statistical software version 3.4.2) | http://www.r-project.org/ | RRID:SCR_001905 |
| GraphPad Prism V7 | https://www.graphpad.com/ | RRID:SCR_002798 |

## RESOURCE AVAILABILITY

### Lead contact

Further information and requests for resources and reagents should be directed to and will be fulfilled by the Lead Contact, Steven M. Chan (steven.chan@uhnresearch.ca).

### Materials availability

This study did not generate new unique reagents.

### Data and code availability

Processed RNA-seq (FKPM) data in Figure 4 is available in Mendeley Data at https://doi.org/10.17632/r6z8xwd945.1. The corresponding pre-processed RNA-seq data has been lost. The expression dataset of *NAMPT* in the different hematopoietic subsets shown in Figure S1 was retrieved from the BloodSpot website (https://servers.binf.ku.dk/bloodspot/). Data for normal hematopoietic cells are from GSE42519. Data for AML cells are from GSE13159.

## EXPERIMENTAL MODEL AND SUBJECT DETAILS

### Human cell lines

All established AML cell lines in this study were authenticated through short-tandem repeat (STR) profiling and periodically tested for mycoplasma contamination using the MycoAlert Mycoplasma Detection Kit (Lonza, Cat # LT07-318) and maintained in RPMI 1640 (Wisent Bioproducts, Cat # 350-035-CL) with 10% (v/v) fetal bovine serum (FBS; Wisent, Cat # 080-150), 2 mM Gluta-Plus (Wisent, Cat # 609-066-EL) and 1mM sodium pyruvate (Wisent, Cat # 600-110-EL). Antimicrobial agents were not added to the culture medium.

Please cite this article in press as: Subedi et al., Nicotinamide phosphoribosyltransferase inhibitors selectively induce apoptosis of AML stem cells by disrupting lipid homeostasis, Cell Stem Cell (2021), https://doi.org/10.1016/j.stem.2021.06.004



OCI-AML-8227 and OCI-AML-21 cells were cultured in X-VIVO 10 medium (Lonza, Cat # 04-380Q) supplemented with 20% (v/v) BIT 9500 serum substitute (Stem Cell Technologies, Cat # 09500), 2 mM Gluta-Plus, and the following cytokines: 10 ng/mL IL-6 (Peprotech, Cat # 200-06), 10 ng/mL IL-3 (Peprotech, Cat # 200-03), 50 ng/mL SCF (Peprotech, Cat # 300-07), 50 ng/mL FLT3L (Peprotech, Cat # 300-19), 10 ng/mL G-CSF (Peprotech, Cat # 300-23) and 25 ng/mL TPO (Peprotech, Cat # 300-18). Antimicrobial agents were not added to the culture medium.

All cell lines were maintained in a humidified incubator at 37°C in 5% $CO_2$.

### Primary AML cells and cord blood HSPCs

Human primary AML samples and cord blood samples were obtained with informed consent according to procedures approved by the University Health Network ethics committee. Primary human AML cells were isolated by differential density centrifugation and cryopreserved in liquid nitrogen. Characteristics of the primary AML samples used in this study are summarized in Table S2. Human HSPCs in cord blood samples were enriched by differential density centrifugation followed by negative depletion of lineage positive cells using magnetic beads (Stem Cell Technologies, Cat # 19356). For short-term *ex vivo* experiments, freshly thawed primary AML cells and cord blood HSPCs were grown in the same medium as OCI-AML-8227 and OCI-AML-21, as described above.

### Mouse studies

All animal experiments were done in accordance with institutional guidelines approved by the University Health Network Animal care committee. Six- to 10-week-old female NOD/SCID/*Il2rg*$^{-/-}$ (NSG) mice were used as hosts for xenotransplantation studies.

## METHOD DETAILS

### Primary and secondary drug screen

The 110 compounds used in the primary screen were dissolved in dimethyl sulfoxide (DMSO) and deposited into 96-well microplates. The master plates were sealed with aluminum foil and stored in −80°C until use. The compounds from the master plates were transferred to wells in 384-well cell culture plates (Sigma, Cat # CLS3571) using an acoustic liquid handler (Echo, Labcyte). The volume of compound transferred in each well was pre-determined to achieve the desired drug concentration in final total volume. Eight serial concentrations were tested for each compound in the primary screen. The concentrations tested for each compound are shown in Table S1. Each well in the 384-well plates were back-filled with DMSO to maintain the same final DMSO concentration in each well. Wells containing DMSO only were included in each plate as controls. Twenty thousand OCI-AML-8227 cells in culture medium were then added to each well in a volume of 80 μl using a robotic dispenser (Multidrop Combi Reagent Dispenser, Thermo Fisher Scientific). The cells were incubated at 37°C in 5% $CO_2$ for 3 days.

After the 3-day incubation, the plates were centrifuged at 500xg for 5 minutes to collect cells at bottom of the plates and the supernatant removed. The cells were resuspended in 10 μL per well of FACS buffer (2% [v/v] FBS in HBSS with calcium) containing 10% (v/v) FcR blocking reagent (Miltenyi Biotech, Cat # 130-059-901), anti-CD34 APC at 1:200 dilution (BD Biosciences, Cat # 340441), anti-CD38 PE at 1:50 dilution (BD Biosciences, Cat # 12-0388-42), Annexin V FITC at 1:20 dilution (BD Biosciences, Cat # 556419), and 7-AAD at 1:20 dilution (BD Biosciences, Cat # 559925). The cells were stained at room temperature for 15 minutes and washed once in FACS buffer. The cells were then fixed in 20 μL per well of fixation buffer (Biolegend, Cat # 420801) for 20 minutes at room temperature and washed once in FACS buffer. The fixed cells were resuspended in 50 μL of freezing medium (10% [v/v] DMSO in FBS) per well. The cell culture plates were then sealed with aluminum foil and stored in −80°C for later analysis. At the time of analysis, the cells were thawed at 37°C for 30 minutes, centrifuged, and resuspended in 60 μL of FACS buffer per well. The cells were analyzed using a BD FACS Canto II flow cytometer with a High Throughout Sampler attachment. The proportion of $CD34^+CD38^-$ cells in the viable population (Annexin $V^-$ and 7-$AAD^-$) was determined for each drug at the different concentrations using FlowJo Software (version 10).

To estimate drug effect, a *t*-statistic was calculated for each drug *i* at concentration *h* using the equation:

$$t_{ih} = \frac{y_{ih} - m}{se_{ih}}$$

, where $y_{ih}$ is the proportion of $CD34^+CD38^-$ cells in a sample treated with drug *i* and concentration *h*, *m* is the mean proportion of $CD34^+CD38^-$ cells in samples treated with DMSO, and $se_{ih}$ is the standard error of the prediction $y_{ih} - m$. The LSC depletion score for each drug *i* was calculated as the mean of the $t_{ih}$ values at the 8 different concentrations tested. The 44 compounds with the lowest LSC depletion scores were selected for confirmation in a secondary screen. The design of the secondary screen was identical to the primary screen except for a greater number of DMSO control wells per plate and an increase in the number of concentrations tested per drug to 10 (Table S1).

### Determination of LSC gene signature

Total RNA was extracted from bulk OCI-AML-8227 cells treated with DMSO or NAMPT inhibitors (Figure 1D) or sorted cell fractions of OCI-AML-21 (Figure S2C). The expression of 104 genes that are differentially expressed between functionally validated LSC+ and LSC- cell fractions was determined in each sample using a custom Nanostring nCounter assay, as previously described (Ng et al., 2016). A $LSC^+$ reference profile was previously defined as the average expression levels of the 104 genes in the $LSC^+$ fractions

Please cite this article in press as: Subedi et al., Nicotinamide phosphoribosyltransferase inhibitors selectively induce apoptosis of AML stem cells by disrupting lipid homeostasis, Cell Stem Cell (2021), https://doi.org/10.1016/j.stem.2021.06.004



(Ng et al., 2016). The similarity of expression of the 104 genes in the test sample to the $LSC^+$ reference profile was determined using a two-tailed Spearman's correlation test. The correlation coefficients are shown on the graphs.

### NSG xenotransplantation

All animal experiments were done in accordance with institutional guidelines approved by the University Health Network Animal care committee. Six- to 10-week-old female NOD/SCID/*Il2rg*$^{-/-}$ (NSG) mice were used as hosts for xenotransplantation studies. All the mice were conditioned with 2.5 gray of irradiation 1 day prior to transplantation.

For Figure 2A, sorted OCI-AML-21 cell fractions were resuspended in Opti-MEM I medium (Thermo Fisher Scientific, Cat # 31985-070) and transplanted into NSG mice by intra-femoral injection. For studies involving OCI-AML-3 cells, the cells were resuspended in Opti-MEM I medium and transplanted into NSG mice by tail vein injection. For studies involving primary human AML samples, the freshly thawed samples were subjected to T cell depletion using anti-CD3 magnetic beads (Stem Cell Technologies, Cat # 17851), resuspended in Opti-MEM I medium, and transplanted into NSG mice by tail vein injection. Cord blood HSPCs were resuspended in Opti-MEM I medium and transplanted into NSG mice by tail vein injection.

### *In vivo* drug treatments

KPT-9274 and its control vehicle formulation were kindly provided by Karyopharm Therapeutics Inc. The drug was resuspended in water at a final concentration of 125 mg/mL. KPT-9274 was administer by oral gavage at the indicated dosing schedule. Control mice were given an equivalent volume of vehicle by oral gavage. Clinical grade dipyridamole was obtained from a hospital pharmacy. The vehicle control formulation was prepared by mixing polyethylene glycol 600 (Sigma, Cat # 8170045000) and tartaric acid (Sigma, Cat # BM0025) in water at a final concentration of 50 mg/mL and 2 mg/mL, respectively. Dipyridamole at a dose of 120 mg/kg per day or an equivalent volume of vehicle was administered by intraperitoneal injection.

### Bone marrow engraftment analysis

Bone marrow cells were collected by aspiration of the femur using a 27-gauge needle. Cell samples were resuspended in RBC Lysis Buffer (Biolegend, Cat # 420301) at room temperature for 5 minutes. The cells were then washed in FACS buffer and stained with the following fluorophore-conjugated antibodies for 30 min at 4°C: anti-mouse TER199 PE-Cy5 at 1:100 dilution, anti-mouse CD45 PE-Cy7 at 1:100 dilution, and anti-human CD45 APC at 1:100 dilution. The SYTOX Green Dead Cell Stain (Thermo Fisher Scientific, Cat # S34859) was used to distinguish dead from live cells. The viable human leukemic population was identified as SYTOX Green$^-$, mTER199$^-$, mCD45$^-$, and hCD45$^+$. To determine the level of CD14 expression on leukemic cells in Figure S3G, the cells were co-stained with an anti-human CD14 PE antibody (BD Biosciences, Cat # 562691) at 1:100 dilution.

### Bioluminescence imaging

Bioluminescence imaging was used to quantify disease burden in NSG mice engrafted with OCI-AML-3 cells modified to express luciferase. Luciferin (PerkinElmer, Cat # 122799) was dissolved in PBS and injected at 150 mg/kg into mice by intraperitoneal injection. The mice were anesthetized by isoflurane, and whole-body bioluminescence imaging of the dorsal view was done at 13 minutes after luciferin injection. Imaging was done using a Xenogen IVIS-200 System. The normalized radiance ($p$/sec/cm$^2$/sr) was recorded for each mouse to quantify leukemic burden.

### Cell viability assessment

Cell viability was measured by staining with Annexin V and propidium iodide (PI). Briefly, the cells were suspended in 1X Annexin binding buffer (Biolegend, Cat # 422201) and stained with Annexin V FITC (Biolegend, Cat # 640945) at 1:20 dilution for 15 minutes at room temperature. PI was then added to the cells at a final concentration of 1μg/mL. For experiments requiring absolute cell quantification, cell counting beads (Thermo Fisher Scientific, Cat # C36995) were used as per manufacturer's instruction.

### Cell cycle analysis

Cells were washed with FACS buffer and stained with anti-CD34 APC and anti-CD38 APC-R700 antibodies for 30 minutes at 4°C. The cells were then washed in PBS and fixed in ice cold 70% (v/v) ethanol for 2 hours. The fixed cells were washed in PBS, treated with RNase A (Gold Biotechnology, Cat # R-050-50), and stained with propidium iodide (PI) for 20 minutes and analyzed on a flow cytometer. The data were analyzed by FlowJo to determine cell cycle status in the CD34$^+$CD38$^-$ population.

### Colony forming unit assay

HSPCs from cord blood or OCI-AML-8227 cells were suspended in MethoCult H4435 Enriched Medium (StemCell Technologies, Cat # 04434) supplemented with nicotinic acid at 100μM. HSPCs were seeded at 500 cells per 1.1 mL. OCI-AML-8227 cells were seeded at 10,000 cells per 1.1 mL. The cell suspensions were divided into aliquots and treated with DMSO or KPT-9274 at the indicated concentration. The cells were plated at a volume of 1.1 mL per dish. The number of colonies formed were counted after 7 days of incubation at 37°C in 5% $CO_2$.

Please cite this article in press as: Subedi et al., Nicotinamide phosphoribosyltransferase inhibitors selectively induce apoptosis of AML stem cells by disrupting lipid homeostasis, Cell Stem Cell (2021), https://doi.org/10.1016/j.stem.2021.06.004





### Western blot

Cells were harvested, washed with PBS, and lysed in RIPA buffer (Sigma, Cat # R0278) supplemented with 1X Halt Protease Inhibitor Cocktail (Thermo Fisher Scientific, Cat # 87786). The samples were incubated on ice for 30 minutes and centrifuged for 20 minutes at 12,000 rpm at 4°C to pellet insoluble material. Protein concentration in the supernatant was measured using the Pierce BCA Protein Assay Kit (Thermo Fisher, Cat # 23227). Equal amounts of protein in 1X LDS sample buffer (Thermo Fisher Scientific, Cat # B0008) were loaded per lane, resolved on a 4 to 12% polyacrylamide gel (Thermo Fisher Scientific, Cat # NW04125BOX), and transferred to a nitrocellulose membrane (Thermo Fisher Scientific, Cat # IB23001). Membranes were blocked with 5% (w/v) BSA in Tris buffered saline with 0.05% (v/v) Tween 20 (TBST) and incubated overnight at 4°C with following primary antibodies in 5% (w/v) BSA in TBST: rabbit anti-NAMPT at 1:1,000 dilution (Cell Signaling Technology, Cat # 61122), mouse anti-NAPRT1 at 1:1,000 dilution (Abcam, Cat # ab211529), mouse anti-SREBP1 at 1:1,000 dilution (Abcam, Cat # ab3259), mouse anti-SCD at 1:1,000 dilution (Cell Signaling Technology, Cat # 2794), rabbit anti-ACSS2 at 1:1,500 dilution (Abcam, Cat # ab66038), rabbit anti-HMGCR at 1:2,000 dilution (Abcam # ab174830), rabbit anti-HMGCS1 at 1:3,000 dilution (Cell Signaling Technology, Cat # 36877), and mouse anti-β-actin at 1:1,000 dilution (Cell Signaling Technology, Cat # 3700). Mouse anti-SREBP2 antibody (BD Biosciences, Cat # 557037) was used at dilution of 1:250 in 5% (w/v) milk in TBST. The membranes were then washed in TBST and probed with IR-Dye 680LT goat anti-mouse (LI-COR Biosciences, Cat # 926-68020) or IR-Dye-800CW goat anti-rabbit (LI-COR Biosciences, Cat # 926-32211) secondary antibodies at 1:10,000 dilution in 5% (w/v) BSA in TBST for 1 hour at room temperature. The membranes were scanned using the Odyssey CLx Imaging system (LI-COR Biosciences).

### Intracellular staining for NAMPT expression

OCI-AML-8227 and OCI-AML-21 cells were washed with FACS buffer and stained with anti-CD34 APC and anti-CD38 APC-R700 antibodies for 30 minutes at 4°C. The cells were washed, resuspended in Fixation/Permeabilization solution (BD Biosciences, Cat # 554714), and incubated at 4°C for 20 min. The fixed cells were then washed, resuspended in 1X Perm/Wash buffer (BD Biosciences, Cat # 554714), and stained with an Alexa Fluor 488-conjugated anti-NAMPT antibody (R&D system, Cat # IC4044G) or an Alexa Fluor 488-conjugated rat IgG2A isotype control antibody (R&D system, Cat # IC006G) for 30 min at 4°C. After staining, the cells were washed twice with 1X Perm/Wash buffer and resuspended in FACS buffer prior to analysis on a flow cytometer.

### NAD quantification by LC/MS

Mass spectrophotometry was used to quantify total NAD levels in OCI-AML-8227 cells. Briefly, OCI-AML-8227 cell fractions were sorted and pelleted by centrifugation. Metabolites from the cell fractions were extracted in a 2:1 mixture of acetonitrile:water and subjected to LC/MS analysis. Ultra pressure liquid chromatography (UPLC) coupled to high resolution accurate mass analysis was performed on a TripleTOF 5600 system in both positive and negative modes. Generic triggering criteria and real time dynamic background subtraction (DBS) algorithm was used during data acquisition to enhance information dependent acquisition (IDA) efficiency. Statistical data processing was performed using MarkerView software and targeted data analysis for endogenous metabolites was processed by PeakView and XIC manager software.

### NAD quantification by colorimetric kit

The NAD/NADH Quantitation Colorimetric Kit (Biovision, Cat # K337-100) was used to quantify total NAD levels in sorted OCI-AML-21 cell fractions. To determine basal NAD levels, OCI-AML-21 cell fractions were sorted, counted, and pelleted by centrifugation at 2,000 rpm for 5 minutes at 4°C. The cell pellets were immediately used for analysis, as per manufacturer's instructions. To determine the effect of KPT-9274 treatment, the sorted cell fractions were resuspended in culture medium and treated with KPT-9274 or DMSO for 24 hours at 37°C. After treatment, the cells were washed in PBS, counted, and pelleted by centrifugation. The cell pellets were immediately used for analysis, as per manufacturer's instructions. The total NAD (NAD+ plus NADH) level in each sample was measured and normalized to input cell number.

### NAD quantification after *in vivo* treatment

Mice engrafted with OCI-AML-3 cells were treated with KPT-9274 for 3 days. After treatment, the mice were sacrificed, and their total bone marrow cells harvested. Human OCI-AML-3 cells in the bone marrow were enriched using the Mouse/Human Chimera Isolation Kit (StemCell Technologies, Cat # 19849). The enriched human cells were immediately pelleted and analyzed for total NAD levels using the NAD/NADH Quantitation Colorimetric Kit described above.

### Metabolomic analysis

THP-1 cells were treated with DMOS or KPT-9274 at 100nM for 24 hours in RPMI-1640 medium supplemented with 10% (v/v) FBS, 2 mM Gluta-Plus, and 1mM sodium pyruvate at 37°C in 5% $CO_2$. After treatment, the cells were collected, washed with PBS, and pelleted by centrifguation. The cell pellets were then snap frozen by liquid nitrogen and submitted for metabolomics analysis. Metabolites were extracted from the frozen cells pellets in a 5:3:2 (v/v/v) mixture of ice-cold methanol:acetonitrile:water at $2 \times 10^6$ cells per mL. After vortexing for 30 minutes at 4°C, the samples were centrifuged at 15,000xg for 10 minutes at 4°C, and 10 μl of supernatants were analyzed by ultra-high pressure liquid chromatography-mass spectrometry (UHPCL-MS) on a Thermo Vanquish UHPLC coupled to a Thermo Q Exactive mass spectrometer using a 5 minute C18 gradient in a positive and negative ion modes (separate runs) exactly as described previously (Gehrke et al., 2019; Nemkov et al., 2019). Peaks areas were integrated using Maven

Please cite this article in press as: Subedi et al., Nicotinamide phosphoribosyltransferase inhibitors selectively induce apoptosis of AML stem cells by disrupting lipid homeostasis, Cell Stem Cell (2021), https://doi.org/10.1016/j.stem.2021.06.004



(Princeton University); metabolite assignment was performed against an in-house standard library as reported (Nemkov et al., 2017).

### Lentiviral vectors encoding shRNAs

Oligonucleotides used to generate shRNA vectors were chemically synthesized by Integrated DNA Technologies. The oligonucleotide sequences are shown in Table S4. The oligos were annealed and inserted into the BbsI cloning site in the Tet-inducible pRSITEP-U6Tet-(sh)-EF1-TetRep-2A-GFP lentiviral vector (Cellecta, Cat # SVSHU6TEP-L).

### Lentiviral production and AML transduction

Lentiviral production and transduction were performed as previously described (Chan et al., 2015). Briefly, 293TN cells were co-transfected with the lentiviral shRNA vector and packaging plasmids, pVSVg and psPAX2, using 293Fectin transfection reagent (Thermo Fisher Scientific, Cat # 12347-019) in 150 mm plates. Supernatants were collected at 48 and 72 hours after transfection. The combined supernatant was centrifuged at 450 x g and filtered through a 0.2 μm PES filter (Thermo Fisher Scientific, Cat # 564-0020). The filtered supernatant (40 mL) was mixed with 10 mL of PBS containing 20% (w/v) PEG 8000 (Sigma, Cat # 89510-1KG-F), incubated overnight at 4°C, and centrifuged at 3,700 rpm for 30 mins at 4°C. The pellet containing lentiviral particles was resuspended in 2 mL of HBSS (Thermo Fisher Scientific, Cat # 14170-112) with 25 mM HEPES (Thermo Fisher Scientific, Cat # 15630-080), aliquoted, and store at −80°C.

For lentiviral transductions, non-TC-treated 24 well plates were coated with 20 μg/mL of Retronectin (Takara, Cat # T100B) for 2 hours at room temperature followed by aspiration and blocking with PBS containing 2% (w/v) BSA (Wisent Bioproducts, Cat # 800-096-EG) for 30 min at room temperature. After aspiration of the blocking buffer, the concentrated virus suspension was added to wells. The plates were then centrifuged at 3,700 rpm for two hours at 4°C to allow virus binding. Following centrifugation, unbound virus was aspirated, and 0.5 to 1x$10^6$ AML cells were added. The plates were then transferred to a 37°C incubator to initiate lentiviral infection.

### RNA sequencing

Total RNA was extracted from OCI-AML-21 cell fractions using the RNeasy Plus Mini Kit (QIAGEN, Cat # 74136) according to manufacturer's instructions. RNA samples were submitted to Novogene Corporation (Sacramento, USA) for sequencing analysis. Briefly, libraries were prepared using the NEBNext® Ultra RNA Library Prep Kit for Illumina, and sequencing was done using the NovaSeq 6000 S4 with PE150 BP sequencing system. STAR (V2.5) software was used to map the reads to reference genome. HTSeq v0.6.1 was used to count the read numbers mapped to each gene. Fragments Per Kilobase Million (FPKM) of each gene was calculated based on the length of the gene and read counts mapped to the gene. Differential expression analysis between two groups was performed using the DESeq2 R package. Genes with an adjusted P value $\leq$ 0.05 found by DESeq2 were assigned as differentially expressed. Gene set enrichment analysis (GSEA) with default parameters was used to identify enriched pathways.

### Real-time quantitative PCR (qPCR)

Total RNA was isolated using the RNeasy Plus Mini Kit (QIAGEN, Cat # 74136). Complementary DNA (cDNA) was synthesized using the iScript Advanced cDNA Synthesis Kit (Bio-Rad, Cat # 1725038). The ADVANCED qPCR mastermix (Wisent Bioproducts, Cat # 800-435-UL) was used to amplify gene targets in the cDNA samples. Sequences of the primer pairs used are shown in Table S5. The CFX96 Touch Real-Time PCR Detection System (Bio-Rad) was used to detect DNA amplification in real time. The delta-delta Ct method was used to determine the relative change in mRNA expression.

### Reactive oxygen species measurements

Lipid ROS were measured by using the C11 BODIPY 581/591 lipid peroxidation sensor (Cayman Chemicals, Cat # 27086). The reagent was directly added to AML cells in growth media to a final concentration of 5μM and incubated at 37°C for 25 minutes. The cells were then washed twice with HBSS, resuspended in 1X Annexin Binding Buffer, and stained with Annexin V conjugated to Alexa Fluor 647 (Thermo Fisher Scientific, Cat # A23204). The ratio of fluorescence at 525/40 (488 nm excitation) to 585/42 (561 nm excitation) in the viable cell population (Annexin V negative) was used to estimate the level of lipid peroxidation.

Cytoplasmic ROS was measured using the CellROX™ Deep Red reagent (Thermo Fisher Scientific, Cat # C10422). The reagent was directly added to AML cells in growth media to a final concentration of 5μM and incubated for 37°C for 25 minutes. The cells were then washed twice with HBSS, resuspended in 1X Annexin Binding Buffer, and stained with Annexin V conjugated to FITC (Biolegend, Cat # 640945). The level of fluorescence emission with a 660/10 filter and 638 nm excitation in the viable cell population (Annexin V negative) was used to estimate the level of cytoplasmic ROS.

Mitochondrial superoxide was measured using the MitoSOX™ Red reagent (Thermo Fisher Scientific, Cat # M36008). The reagent was directly added to AML cells in growth media to final concentration of 5μM and incubated for 37°C for 25 minutes. The cells were then washed twice with HBSS, resuspended in 1X Annexin Binding Buffer, and stained with Annexin V conjugated to Alexa Fluor 647 (Thermo Fisher Scientific, Cat # A23204). The level of fluorescence emission with a 585/42 filter and 488 nm excitation in the viable cell population (Annexin V negative) was used to estimate the level of mitochondrial superoxide.

### Active caspase 3/7 assay

Active caspases 3/7 was measured using the FAM-FLICA Caspase 3/7 Assay kit (Bio-Rad, Cat # ICT093) as per manufacturer's instructions. Briefly, the FAM-FLICA reagent was directly added to AML cells in growth media and incubated for 40 minutes at 37°C.

Please cite this article in press as: Subedi et al., Nicotinamide phosphoribosyltransferase inhibitors selectively induce apoptosis of AML stem cells by disrupting lipid homeostasis, Cell Stem Cell (2021), https://doi.org/10.1016/j.stem.2021.06.004





The cells were then washed and resuspended in FACS buffer with propidium iodide (PI). The level of fluorescence emission with a 525/30 filter and 488 nm excitation in the PI negative population was used to estimate the proportion of cells in early apoptosis with active caspase 3 and 7.

## QUANTIFICATION AND STATISTICAL ANALYSIS

Statistical analysis between groups was performed as indicated in figure legends using R and GraphPad Prism v7. Number of times the experiments were repeated or the number of animals in each group are indicated in figure legends. Statistical significance of survival curve was determined by Log-rank (Mantel-Cox) test. P values less than 0.05 were considered significant. Relative protein quantification from western blot images were done by ImageStudio using Odyssey CLx Imaging system (LI-COR Biosciences).